CHEMISTRY
A EUROPEAN JOURNAL

DOI: 10.1002/chem.200800460

Non-natural Amino Acids as Modulating Agents of the Conformational Space of Model Glycopeptides

Alberto Fernández-Tejada, Francisco Corzana,* Jesús H. Busto, Gonzalo Jiménez-Osés, Jesús M. Peregrina,* and Alberto Avenoza[a]

Abstract: The synthesis and conformational analysis in aqueous solution of different α-methyl-α-amino acid diamides, derived from serine, threonine, β-hydroxycyclobutane-α-amino acids, and their corresponding model β-*O*-glucopeptides, are reported. The study reveals that the presence of an α-methyl group forces the model peptides to adopt helix-like conformations. These folded conformations are especially significant for cyclobutane derivatives. Interestingly, this feature was also observed in the corresponding model glucopeptides, thus indicating that the α-methyl group and not the β-*O*-glucosylation process largely determines the conformational preference of the backbone in these structures. On the other hand, atypical conformations of the glycosidic linkage were experimentally determined. Therefore, when a methyl group was located at the Cβ atom with an *R* configuration, the glycosidic linkage was rather rigid. Nevertheless, when the *S* configuration was displayed, a significant degree of flexibility was observed for the glycosidic linkage, thus showing both alternate and eclipsed conformations of the ψ_s dihedral angle. In addition, some derivatives exhibited an unusual value for the ϕ_s angle, which was far from a value of −60° expected for a conventional β-*O*-glycosidic linkage. In this sense, the different conformations exhibited by these molecules could be a useful tool in obtaining systems with conformational preferences "à la carte".

Keywords: amino acids · conformation analysis · glycopeptides · molecular dynamics · NMR spectroscopy

Introduction

Glycoproteins and glycopeptides are involved in fundamental biological processes in which the carbohydrate and the sequence of the amino acids frequently have different and complex biological functions.[1]

The most common *O*-glycosylations involve the α-*O*-glycosidic linkage of *N*-acetylgalactosamine (GalNAc) attached to a rich domain of serine (Ser) and/or threonine (Thr) residues (mucin-type)[2] or the β-*O*-glycosidic linkage of *N*-acetylglucosamine (GlcNAc) linked to a Ser/Thr residue of cytoplasmic and nuclear proteins, which play a regulatory role in protein function.[3] In contrast, some specific types of *O*-glycosylation, such as the β-*O*-linked attachment of D-glucose (Glc) to Ser/Thr (*O*-glucosylation), are less frequent and have been found in the epidermal growth factor (EGF) domains of different serum proteins[4] and Notch receptor.[5] The role of the Glc moiety in these systems is unknown and remains controversial. However, it is essential to know the influence that the carbohydrate moiety has on the conformational equilibrium of the peptide backbone and vice versa. In this context, we have recently reported that the β-*O*-glucosylation of model peptides derived from Ser and Thr allows the backbone to expand its conformational space, thus exhibiting not only extended but also folded conformations.[6]

On the other hand, one attractive approach to the detailed study of the influence that distinct structural elements have on the conformational preferences of a molecule is to design novel glycopeptides in which natural amino acids have been replaced with non-natural amino acids. In addition, the resulting novel glycopeptides could stabilize one conformation (i.e., the bioactive conformation) or could exhibit conformers that have rarely been observed in the natu-

[a] A. Fernández-Tejada, Dr. F. Corzana, Dr. J. H. Busto, Dr. G. Jiménez-Osés, Dr. J. M. Peregrina, Dr. A. Avenoza
Departamento de Química
Universidad de La Rioja
UA-CSIC 26006 Logroño (Spain)
Fax: (+34) 941-299-621
E-mail: francisco.corzana@unirioja.es
jesusmanuel.peregrina@unirioja.es

Supporting information for this article is available on the WWW under http://www.chemeurj.org/ or from the author.

ral derivatives, thus modifying the binding to the target molecules. In this sense, although the synthesis of non-proteinogenic α-amino acids has received enormous attention, particularly α,α-disubstituted α-amino acids,[7] the field of modified glycosyl-α-amino acids remains relatively unexplored. Most of the modifications are centered around the saccharide moiety[8] and rarely on the peptide moiety.[9] As a consequence, the glycosylation of novel β-hydroxy-α,α-disubstituted amino acids[10] could be a useful tool in the design of molecules with a novel conformational behavior regarding the natural compounds.

On this basis, we report herein the synthesis and the conformational analysis in aqueous solution of different model peptides derived from non-natural amino acids and the corresponding model β-*O*-glucopeptides (Scheme 1). In these models, the amino and carboxylic functional groups were transformed into amides to simulate the peptide backbone. The main goal of this study was to investigate in detail the effects that the substituents at the Cα and/or Cβ atoms have on the peptide backbone, the lateral chain, and the glycosidic linkage conformational preferences.

The study involved the use of distance information based on NOE interactions and coupling constants, which were interpreted with the assistance of molecular-dynamics (MD) simulations. It is important to note that not only was the synthesis of the non-natural target compounds difficult, as

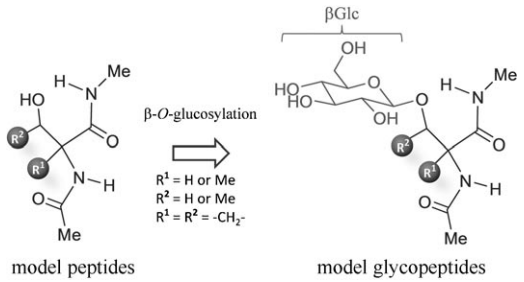

Scheme 1. Design of novel β-*O*-glucopeptides derived from non-natural amino acids.

the α-amino acid derivatives bear quaternary carbon atoms, but their structural analysis was also extremely complicated. Indeed, the absence of the Hα atom in the α-substituted α-amino acid derivatives implicates the lack of some NOE interaction signals and coupling constants, which are pivotal keys in eliciting the conformations. Moreover, the computational studies of these systems are not trivial. Indeed, the currently used all-atom force fields that predict reasonable conformational dynamics for larger peptides or proteins fail to reproduce the measured conformational distributions for di- and tripeptide systems.[11] In addition, the use of general force fields, which have not been tested for all types of organic molecules, is required for the study of non-natural amino acids.

Abstract in Spanish: *En este artículo se presenta la síntesis y el análisis conformacional en disolución acuosa de diferentes diamidas de α-metil-α-aminoácidos derivados de Ser, Thr y β-hidroxiciclobutan-α-aminoácidos, así como de sus correspondientes β-O-glucopéptidos modelo. El estudio reveló que la presencia de un grupo metilo en posición α del aminoácido fuerza al péptido modelo a adoptar conformaciones plegadas de tipo hélice. Estas conformaciones plegadas son especialmente significativas para los derivados que incorporan la estructura de ciclobutano. Esta característica también fue observada para los correspondientes glucopéptidos modelo, lo cual indica que es el grupo metilo en posición α y no la β-O-glucosilación lo que determina en gran medida las preferencias conformacionales de la cadena peptídica en estas estructuras. Por otro lado, se observaron experimentalmente conformaciones atípicas del enlace glicosídico. Así, cuando un grupo metilo está localizado en el Cβ con configuración R, el enlace glicosídico es bastante rígido. Sin embargo, cuando dicho carbono muestra configuración S se observa un alto grado de flexibilidad en el enlace glicosídico, mostrando el ángulo diedro ψ_s tanto conformaciones alternadas como eclipsadas. Además, algunos derivados exhibieron valores inusuales del ángulo diedro ϕ_s, los cuales se apartan bastante del valor esperado de −60° para un enlace β-O-glicosídico convencional. En este sentido, las diferentes conformaciones exploradas por estas moléculas podrían ser utilizadas como herramientas útiles para obtener sistemas con preferencias conformacionales "à la carte".*

Results and Discussion

Synthesis: Scheme 2 shows all the model peptides and glycopeptides studied herein. Compounds Ac-L-Ser-NHMe, Ac-L-(β-*O*-D-Glc)Ser-NHMe (referred to as Ac-L-Ser*-NHMe), Ac-L-Thr-NHMe, and Ac-L-(β-*O*-D-Glc)Thr-NHMe (referred to as Ac-L-Thr*-NHMe) were previously synthesized and studied by us.[6] The α-methylated compound was derived from α-methylserine (MeSer), the α,β-dimethylated compounds from α-methylthreonine (MeThr), and the cyclobutane derivatives from 2-hydroxy-1-aminocyclobutanecarboxylic acid (c_4Ser).

The synthesis of the model peptides was carried out as described in the Supporting Information. The corresponding model glycopeptides were obtained under the modified conditions of the Koenigs–Knorr glycosylation.[12] Scheme 3 shows the synthesis of Ac-(*S*)-MeSer*-NHMe, Ac-(*R*,*R*)-MeThr*-NHMe, Ac-(*S*,*S*)-c_4Ser*-NHMe, and Ac-(*R*,*R*)-c_4Ser*-NHMe as representative examples of non-natural model glycopeptides. The syntheses of the rest of the model glycopeptides are described in the Supporting Information.

Glycopeptide Ac-(*S*)-MeSer*-NHMe was synthesized from derivative **1**, which has been previously glycosylated by our group[13] to give **2**. Further deprotection of the carboxylic acid and subsequent reaction with methylamine led to **4**. Finally, the transformation of the azide group into the amine group with H_2 and Pd/C as a catalyst, followed by

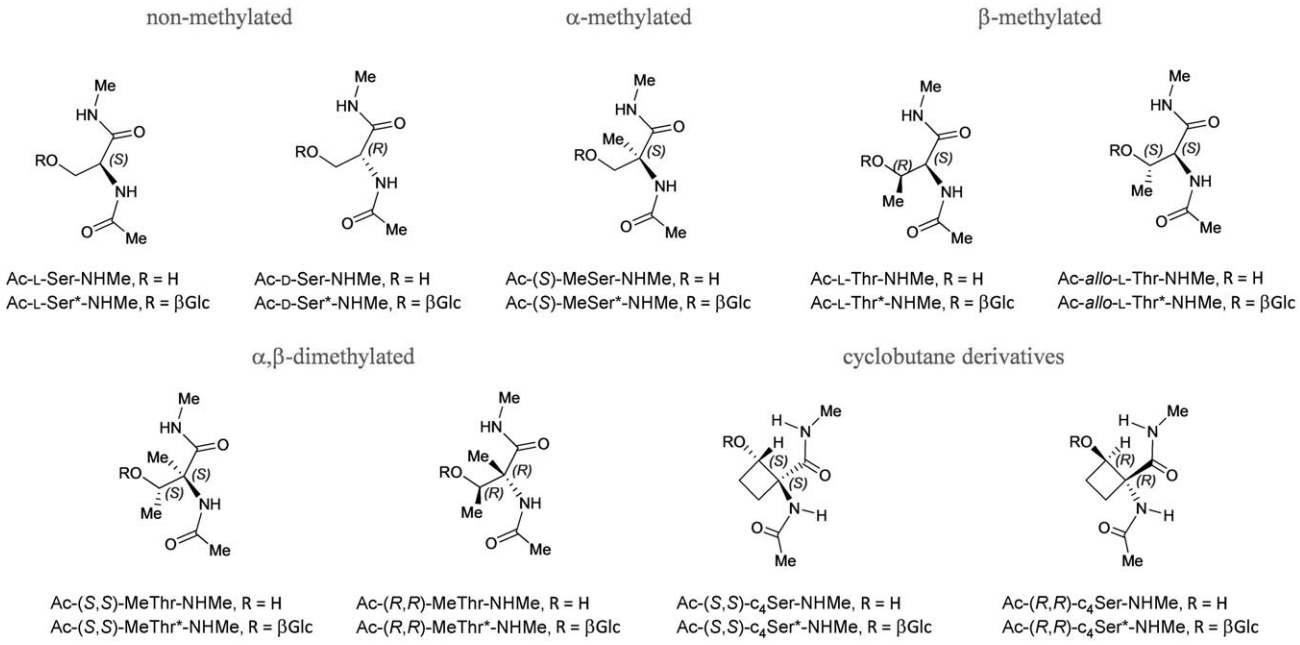

Scheme 2. Model peptides and glycopeptides studied herein.

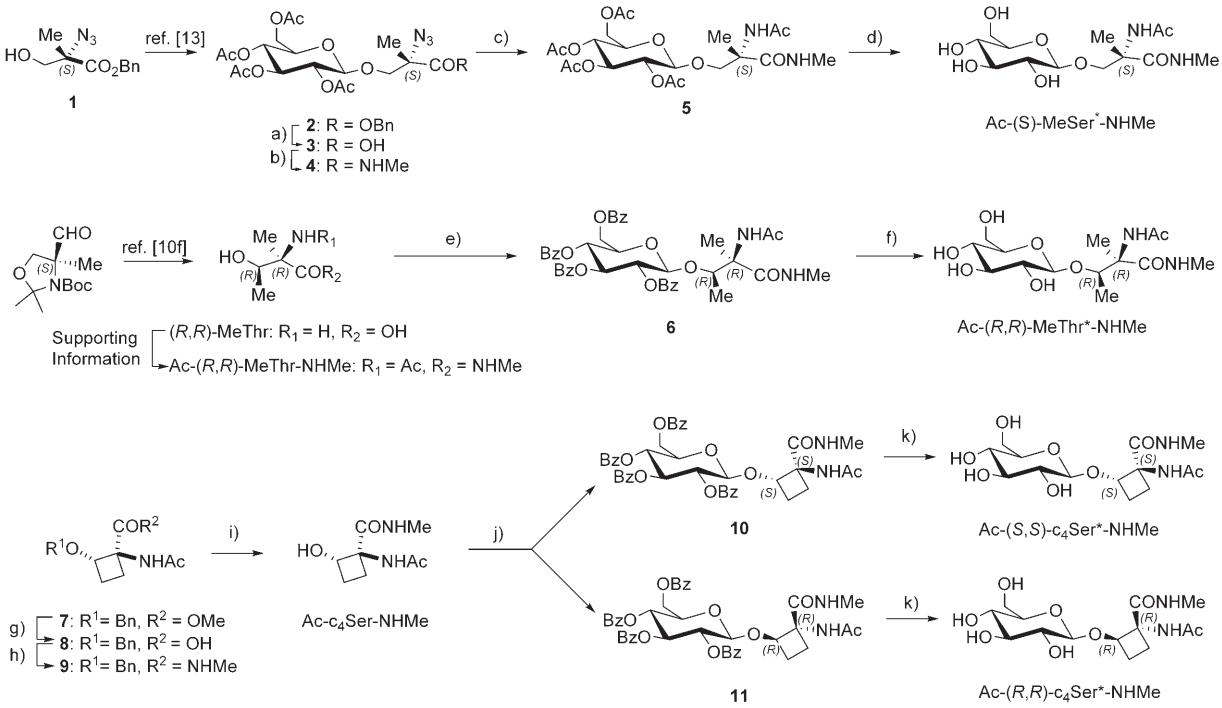

Scheme 3. Synthetic route to model glycopeptides Ac-(*S*)-MeSer*-NHMe, Ac-(*R*,*R*)-MeThr*-NHMe, Ac-(*S*,*S*)-c$_4$Ser*-NHMe, and Ac-(*R*,*R*)-c$_4$Ser*-NHMe. a) H_2, Pd/C, AcOEt, 25 °C 16 h (90 %); b) $MeNH_2$·HCl, TBTU, DIEA, CH_3CN 25 °C 16 h (84 %); c) i. H_2, Pd/C MeOH 25 °C 15 h; ii. Ac_2O, pyridine, 25 °C 4 h (77 %); d) MeONa/MeOH 25 °C 3 h (90 %); e) described in the Supporting Information; f) MeONa/MeOH, 25 °C, 3 h (87 %); g) LiOH·H_2O, MeOH/H_2O (3:1), 25 °C, 12 h (97 %); h) $MeNH_2$·HCl, TBTU, DIEA, MeCN, 25 °C, 10 h (92 %); i) H_2, Pd/C, MeOH, 1 atm, 25 °C, 12 h (99 %); j) i. 2,3,4,6-tetra-*O*-benzoyl-α-D-glucopyranosyl bromide, AgTfO, CH_2Cl_2, −30–25 °C, 4-Å MS, 15 h (30 %; **10**+**11**); ii. column chromatography (dichloromethane/MeOH 9.5:0.5); k) MeONa/MeOH, 25 °C, 3 h (92 % for Ac-(*S*,*S*)-c$_4$Ser*-NHMe and 85 % for Ac-(*R*,*R*)-c$_4$Ser*-NHMe). MS = molecular sieves.

acetylation and subsequent deprotection gave glycopeptide Ac-(*S*)-MeSer*-NHMe.

On the other hand, the model glycopeptide Ac-(*R*,*R*)-MeThr*-NHMe was obtained from the model peptide Ac-(*R*,*R*)-MeThr-NHMe, which was prepared according to the

procedure described in the Supporting Information from the amino acid (*R*,*R*)-MeThr, the synthesis of which has been previously reported.[10f] The treatment of model peptide Ac-(*R*,*R*)-MeThr-NHMe with 2,3,4,6-tetra-*O*-benzoyl-α-D-glucopyranosyl bromide in the presence of silver trifluoromethanesulfonyl (AgOTf) gave derivative **6**, which was further deprotected to afford the model glycopeptide Ac-(*R*,*R*)-MeThr*-NHMe.

In the case of the cyclobutane derivatives Ac-(*S*,*S*)-c$_4$Ser*-NHMe and Ac-(*R*,*R*)-c$_4$Ser*-NHMe, the synthesis started from a racemic mixture of compound **7**, which was recently synthesized by our group.[10j] Later, the hydrolysis of the methyl ester with LiOH·H$_2$O gave the corresponding acid **8** in an almost quantitative manner (97%). Further treatment with MeNH$_2$·HCl and *N*,*N*,*N*′,*N*′-tetramethyl-*O*-(benzotriazol-1-yl)uronium tetrafluoroborate (TBTU) as a coupling agent in the presence of diisopropylethylamine (DIPEA) as a base afforded diamide **9**. Final hydrogenolysis with H$_2$ and Pd/C quantitatively removed the benzyl group, thus leading to the desired Ac-c$_4$Ser-NHMe as a racemic mixture. The treatment of Ac-c$_4$Ser-NHMe with 2,3,4,6-tetra-*O*-benzoyl-α-D-glucopyranosyl bromide in the presence of AgOTf exclusively gave β-anomers **10** and **11**, which were separated by column chromatography on silica gel, in a moderate yield. Finally, the deprotection of the hydroxy groups of the carbohydrate moiety with NaOMe gave the corresponding model glycopeptides Ac-(*S*,*S*)-c$_4$Ser*-NHMe and Ac-(*R*,*R*)-c$_4$Ser*-NHMe.

To unambiguously confirm the absolute configuration of compounds Ac-(*S*,*S*)-c$_4$Ser*-NHMe and Ac-(*R*,*R*)-c$_4$Ser*-NHMe, acid derivative **8** was treated with ethyl-3-(3-dimethylamino)propylcarbodiimide hydrochloride salt (EDCI·HCl) as a coupling agent and 4-dimethylaminopyridine (DMAP) as a base to give **12** in an 87% yield (Scheme 4). Oxazolone **12** was then transformed into esters **13** and **14** by reaction with (*S*)-(−)-1-(2-naphtyl)ethanol in the presence of KO*t*Bu as a base. The ester compounds were separated by column chromatography on silica gel, thus obtaining **14** in a pure form (6% yield from **12**). We were able to obtain single crystals of **14** by slow evaporation of a solution of this compound in hexane and dichloromethane. The new stereogenic centers were found to have a *R*,*R* configuration. Finally, the deprotection of ester moiety in **14** with LiOH·H$_2$O gave (*R*,*R*)-**8**, which was converted into Ac-(*R*,*R*)-c$_4$Ser*-NHMe following the reactions given above.

Conformational study of model peptides: The torsional angles and the labeling of the atoms used herein for the compounds are shown in Figure 1. In a first step, full assignment of the protons in all of the compounds was carried out using COSY and HSQC experiments. Then, selective 1D NOESY experiments in D$_2$O (see the Supporting Informa-

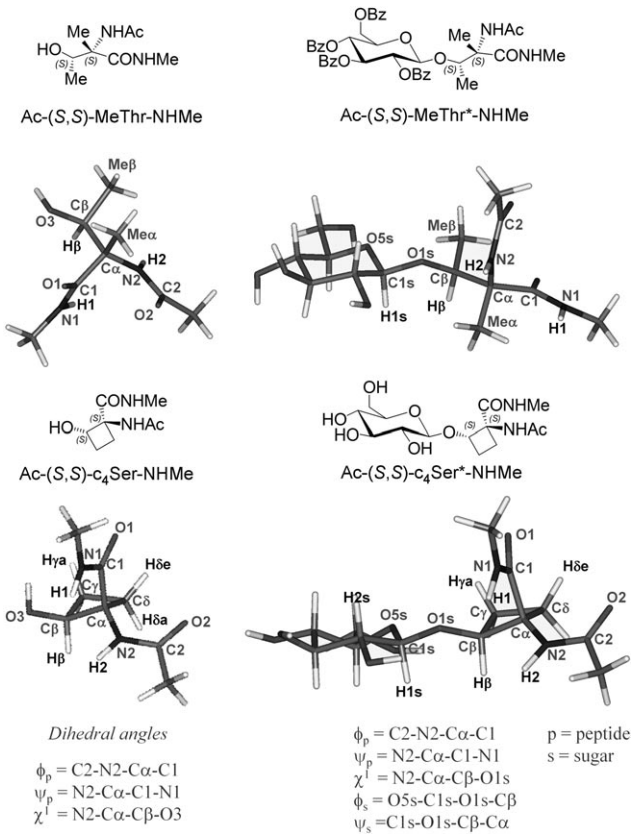

Figure 1. Molecular structures of Ac-(*S*,*S*)-MeThr-NHMe, Ac-(*S*,*S*)-MeThr*-NHMe, Ac-(*S*,*S*)-c$_4$Ser-NHMe, and Ac-(*S*,*S*)-c$_4$Ser*-NHMe showing the definitions of the torsional angles and the atom labeling. The same definitions were used for all the molecules studied herein.

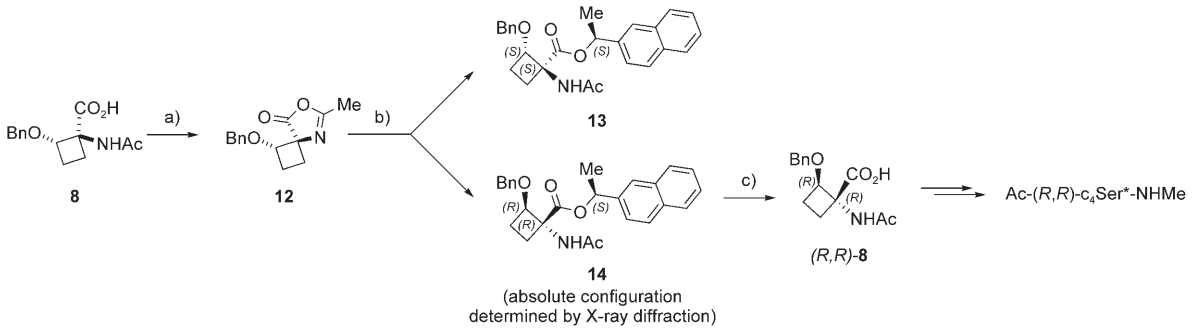

Scheme 4. Determination of the absolute configuration of glycopeptides Ac-(*S*,*S*)-c$_4$Ser*-NHMe and Ac-(*R*,*R*)-c$_4$Ser*-NHMe. a) EDCI·HCl, DMAP, CH$_2$Cl$_2$, 25 °C 2 h (87%); b) i. (*S*)-(−)-1-(2-naphtyl)ethanol, *t*BuOK, THF, 25 °C, 12 h (70%); ii. column chromatography (hexane/ethyl acetate, 4:6) to obtain **14** in a pure form; c) LiOH·H$_2$O, MeOH/H$_2$O (3:1), 25 °C, 4 d (96%).

tion) and 2D NOESY experiments (see Figure 2 and the Supporting Information) in H_2O/D_2O (9:1) were carried out for all the compounds. In addition, $^3J(H_\alpha,H_\beta)$ and $^3J(NH_2,H_\alpha)$ coupling constants were measured in the case of natural amino acid derivatives.

Although the model peptides studied herein are too short to adopt a defined secondary structure, the NOESY data can still be used to assess "conformational preferences". This behavior is based on the observation of key sequential NH–NH ($i,i+1$) and Hα–NH ($i,i+1$) connectivities. Consequently, the observation of strong Hα-NH ($i,i+1$) NOE interactions along with weak or absent NH–NH ($i,i+1$) NOE interactions suggests a conformational preference for extended conformations. On the contrary, the observation of weak–medium Hα–NH ($i,i+1$) NOE interactions and strong NH–NH ($i,i+1$) NOE interactions suggests a conformational preference for helical dihedral space.[14]

Figure 2 (upper panel) shows the amide region of the 2D NOESY spectra of model peptides Ac-*allo*-L-Thr-NHMe, Ac-(*S*)-MeSer-NHMe, and Ac-c_4Ser-NHMe as representative cases. As reported for peptides derived from natural Ser and Thr[6] (i.e., Ac-L-Ser-NHMe and Ac-L-Thr-NHMe, respectively), the 2D NOESY spectrum of the (*S*)-*allo*-threonine derivative (compound Ac-*allo*-L-Thr-NHMe) displayed a strong Hα–NH1 NOE interaction and the absence of the NH1–NH2 NOE interaction, which suggests a conformational preference for extended-like conformations.[14] On the contrary, the medium NH1–NH2 NOE interaction observed in derivatives Ac-(*S*)-MeSer-NHMe and Ac-c_4Ser-NHMe could indicate the presence of an significant population of the helix-like conformations (see the Supporting Information).

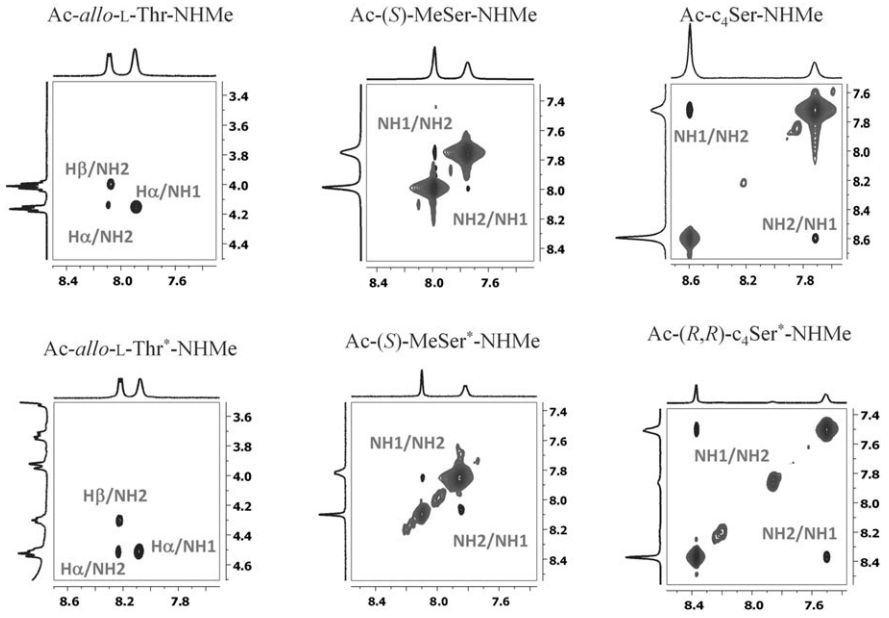

Figure 2. Section of the 800 ms 2D NOESY spectrum (400 MHz) in H_2O/D_2O (9:1) at 25 °C of different peptides (upper panel) and glycopeptides (lower panel) studied herein. For the α-methylated and cyclobutane derivatives, the amide–amide cross-peaks region is shown. The diagonal peaks are negative. The NOE interactions are represented as positive cross-peaks.

As a first step in deducing the conformational behavior of these molecules, relaxed potential-energy maps were calculated for all the compounds using the AMBER94, CHARMM, and MM+ force fields as described in the Experimental Section. These surfaces just provide a first estimation of the conformational regions that are energetically accessible for each compound (see Figure 3a and the Supporting Information). As shown in Figure 3a, the potential-energy surface calculated with, for example, the CHARMM force field for Ac-(*S*)-MeSer-NHMe shows the presence of four minima, referred to as α_D (with ϕ_p close to −60° and ψ_p around −60°), α_L (characterized by ϕ_p close to 60° and ψ_p around 60°), polyproline type II (PPII; with ϕ_p close to −60° and ψ_p around 180°), and an unusual conformation for natural amino acids (ϕ_p close to 60° and ψ_p around −180°), denoted as F* according to the definition used previously.[15]

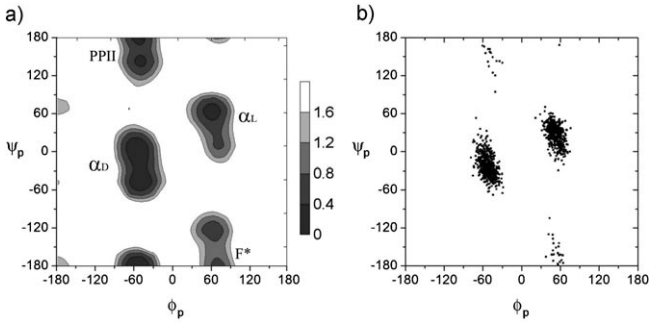

Figure 3. a) Potential-energy surfaces calculated with the CHARMM force field for Ac-(*S*)-MeSer-NHMe. b) ϕ_p/ψ_p distribution obtained from 10 ns unrestrained MD simulations in explicit water (298 K, 1 atm, TIP3P water molecules, boundary conditions, and Ewald sums for the treatment of electrostatic interactions) for Ac-(*S*)-MeSer-NHMe.

The next and most important step in the conformational analysis of the molecules was to get an ensemble that could reproduce our experimental NMR spectroscopic data. As stated above, the unrestrained MD simulations carried out on small systems normally fail to reproduce the conformational behavior of the peptide backbone. In particular, the AMBER94 force field used in our MD simulations shows a clear tendency to overestimate the helix-like conformations (see Figure 3b and the Supporting Information). Consequently, the relative population of conformers obtained

from the unrestrained MD simulations of the peptide backbone is not in good agreement with the experimental NMR spectroscopic data. On the other hand, it is important to note that the direct interpretation of NOE interaction data in flexible molecules in terms of a single structure may lead to the generation of high-energy virtual conformations.[16] Therefore, and following our previously reported protocol,[6,17] we combine herein the NMR spectroscopic data with time-averaged restrained MD (MD-tar) simulations with the objective of obtaining a distribution of low-energy conformers (according to the AMBER force field) able to quantitatively reproduce the NMR spectroscopic data. This procedure overcomes the limitations inherent in both techniques (NMR spectroscopic analysis and MD simulations) and provides a simple and robust way to consider the flexibility of the molecule in the interpretation of the NMR spectroscopic data.

Consequently, proton–proton distances were experimentally determined from the corresponding NOE interaction build-up curves[18] (see the Supporting Information) and distances involving NH protons were semiquantitatively determined by integrating the volume of the corresponding cross peaks. These data together with the ^3J coupling constants[19] were used as restraints in MD-tar analysis.[20] The distribution for the peptide backbone ϕ_p/ψ_p of the model peptides obtained from the MD-tar simulations is shown in Figure 4. It is important to note that the MD-tar simulation of Ac-(*S*)-MeSer-NHMe now explores the four conformations shown in Figure 3a, with relative populations in accordance with the experimental NMR spectroscopic data (see Figure 4b and the Supporting Information). According to the NOE interaction experiments mentioned above, the ϕ_p/ψ_p dihedral values (backbone) of Ac-*allo*-L-Thr-NHMe were characteristic of extended conformations, such as PPII and the β sheet, and only a small number of conformers (ca. 11%) showed ϕ_p/ψ_p dihedral values that correspond to an α-helical conformation. This result is very similar to that previously found for Ac-L-Ser-NHMe and Ac-L-Thr-NHMe derivatives.[6]

On the other hand, the model peptides derived from α,α-disubstituted amino acids (i.e., Ac-(*S*)-MeSer-NHMe, Ac-(*S*,*S*)-MeThr-NHMe, and Ac-c_4Ser-NHMe) showed a significant population of conformers with ϕ_p/ψ_p dihedral values characteristic of helix-like conformations. Figure 5 indicates

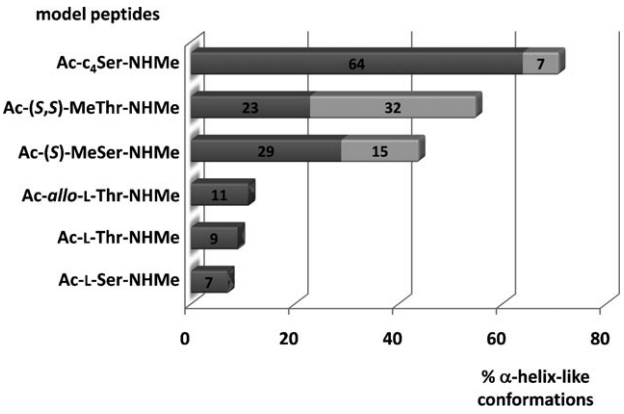

Figure 5. Total helix-like population (dark gray: α_D; light gray: α_L) obtained for the model peptides from the MD-tar simulations.

the total number of α helix-like conformations $\alpha_D+\alpha_L$ present in the model peptides in aqueous solution. In the case of Ac-(*S*)-MeSer-NHMe and Ac-(*S*,*S*)-MeThr-NHMe, the α_D and α_L conformers coexist with extended conformations, such as PPII and F*. It is important to mention that these four major conformers found for Ac-(*S*)-MeSer-NHMe lie at the local minima previously calculated for model peptide Ac-(*S*)-MeSer-NHMe.[21] The cyclobutane ring significantly promoted the helix-like structures ($\alpha_D \approx 64\%$), in good accordance with the results previously described by others.[22] Additionally, the MD simulations carried out on the cyclobutane derivative suggest the existence of approximately 17% of the γ-turn conformation (γ_D).

In this case, the same conformational preference for the backbone of Ac-c_4Ser-NHMe was observed in the solid state with $\phi_p=-84.4°$ and $\psi_p=-7.8°$ (Figure 6). Moreover, the molecule adopts only one ring-puckering conformation in the solid state, with the pucker angle θ close to $-23.9°$ and with the substituent at the Cβ atom in an equatorial position, which is similar to that previously described by us for other cyclobutane derivatives.[23] In the same way, a single ring-puckering conformation was found in aqueous solution, as deduced from the MD-tar simulations, with $\theta=-20.3°$. As we have reported,[23] the existence of a single ring-puckering conformation is entirely compatible with the experi-

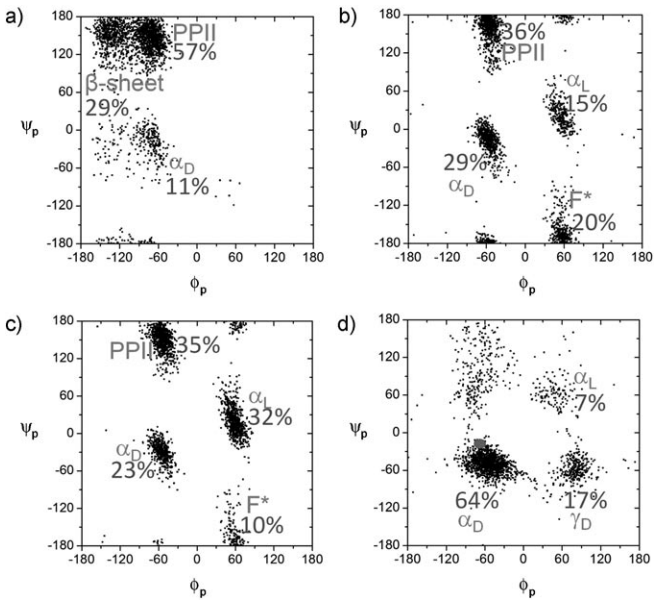

Figure 4. Distribution of the peptide backbone (ϕ_p/ψ_p) of the model peptides obtained from the MD-tar simulations: a) Ac-*allo*-L-Thr-NHMe, b) Ac-(*S*)-MeSer-NHMe, c) Ac-(*S*,*S*)-MeThr-NHMe, and d) Ac-c_4Ser-NHMe. For Ac-c_4Ser-NHMe, the conformation of the backbone in the solid state is shown as a grey circle.

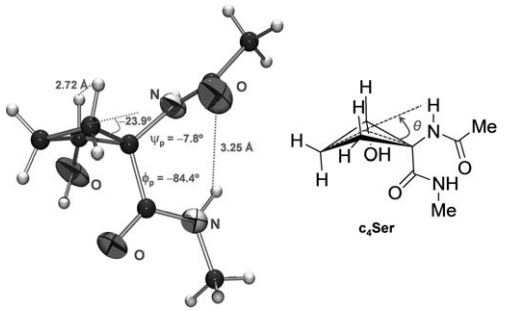

Figure 6. Some geometrical features of the crystal structure of Ac-c_4Ser-NHMe and the pucker angle θ.

mentally determined distance Hβ–Hδa of 2.7 Å (experimentally determined from the NOE interaction build-up curves).

As far as the lateral chain is concerned, its conformational behavior is characterized by the χ^1 torsional angle, which can adopt three lowest-energy staggered rotamers, denoted as *gauche*(−) or *g*(−)($\chi^1 \approx -60°$), *gauche*(+) or *g*(+)($\chi^1 \approx 60°$), and *anti* or *t*($\chi^1 \approx -180°$; Figure 7a).

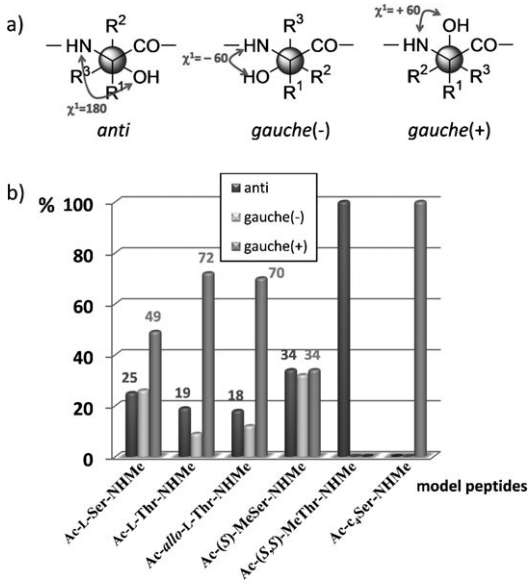

Figure 7. a) More stable conformers of the lateral chain χ^1. b) χ^1 distributions obtained from the MD-tar simulations for the different model peptides. Angle χ^1 is around 105° for Ac-c_4Ser-NHMe.

Figure 7b shows the population of the χ^1 angle obtained from the MD-tar simulations for the model peptides. A number of points warrant particular attention. Model peptides derived from the natural L-Ser and L-Thr showed a conformational preference for the χ^1 angle close to 60°. Furthermore, and as a result of the steric requirements of the β-methyl group of Thr, the population of *gauche*(+) is slightly higher in Ac-L-Thr-NHMe (ca. 72%). Markedly, a similar result was obtained for derivative Ac-*allo*-L-Thr-NHMe, in which the Cβ atom has the opposite configuration. In contrast, the α-methylated derivative Ac-(*S*)-MeSer-NHMe exhibited a rather flexible behavior for the χ^1 angle. On the other hand, for the α- and β-methylated compound Ac-(*S*,*S*)-MeThr-NHMe the lateral chain is rather rigid and displays only the *anti* conformation. Finally, the cyclobutane derivative Ac-c_4Ser-NHMe presented a rigid lateral chain as a result of the restriction imposed by the four-membered ring. Indeed, the χ^1 angle has a value of around 105° throughout the MD simulation.

Conformational study of model glycopeptides: As a first step and following the protocol previously described for the model peptides, the relaxed potential-energy maps were calculated for all the glycopeptides using the AMBER94, CHARMM, and MM+ force fields. Figure 8a shows the potential-energy map calculated for Ac-(*S*,*S*)-MeThr*-NHMe with the CHARMM force field. Alternatively, and to explore the conformational behavior of these molecules, 100 ns unrestrained MD simulations in a vacuum at 400 K were carried out for all the glycopeptides (see Figure 8b and the Supporting Information). In this case, the high temperature avoids kinetically trapping the molecules in some local minima (Figure 8b). As can be seen for glycopeptide Ac-(*S*,*S*)-MeThr*-NHMe, this simulation explores all the minima found by the CHARMM force field (compare Figure 8a and b). As in the case of the peptides, the unrestrain-

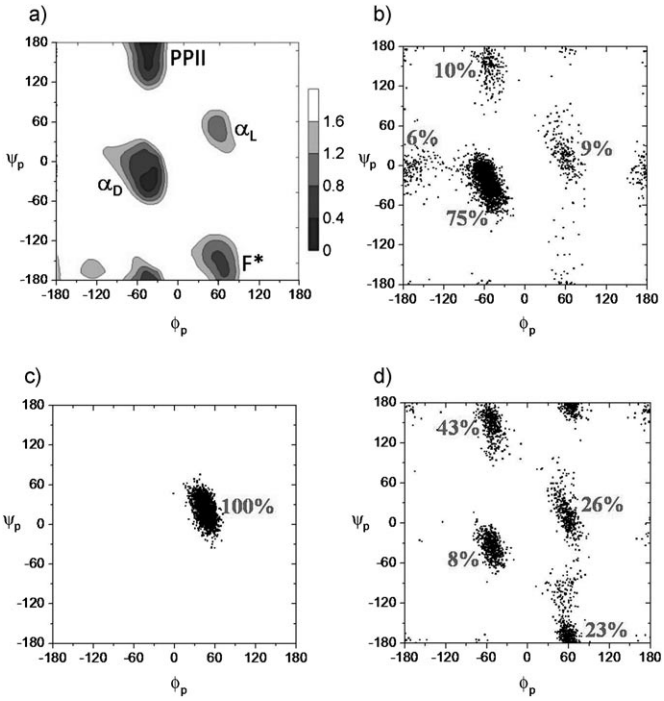

Figure 8. a) Potential-energy surfaces calculated with the CHARMM force field for Ac-(*S*,*S*)-MeThr*-NHMe. b) ϕ_p/ψ_p distribution obtained from 100 ns unrestrained MD simulations in a vacuum at 400 K for Ac-(*S*,*S*)-MeThr*-NHMe. c) ϕ_p/ψ_p distribution obtained from 10 ns unrestrained MD simulations in explicit water (298 K, 1 atm, TIP3P water molecules, boundary conditions, and Ewald sums for the treatment of electrostatic interactions) for Ac-(*S*,*S*)-MeThr*-NHMe. d) ϕ_p/ψ_p distribution obtained from the MD-tar simulations for Ac-(*S*,*S*)-MeThr*-NHMe.

ed MD simulation carried out in explicit water at 298 K failed to reproduce the conformational behavior of the peptide backbone. Thus, for Ac-(*S*,*S*)-MeThr*-NHMe only one of the minimum was populated, namely the α_L conformer (Figure 8c). In contrast, the inclusion of the NMR spectroscopic data (proton–proton distances and ^3J coupling constants) as restraints in the MD-tar simulations gave a ϕ_p/ψ_p distribution that can quantitatively reproduce the experimental data (see Figure 8d and the Supporting Information).

The 2D NOESY pattern spectra corresponding to the model glycopeptides is, in all cases, rather similar to those obtained for their parent peptides (see the lower panel of Figure 2 and the Supporting Information). Consequently, a ϕ_p/ψ_p distribution comparable to the distribution obtained for the peptides could be expected. That is, the β-*O*-glucosylation does not have a significant effect upon the conformation of the peptide backbone in the case of non-natural amino acids.

The percentages of helix-like conformation for model glycopeptides Ac-D-Ser*-NHMe and Ac-*allo*-L-Thr*-NHMe were calculated to be 12 and 11%, respectively (Figure 9).

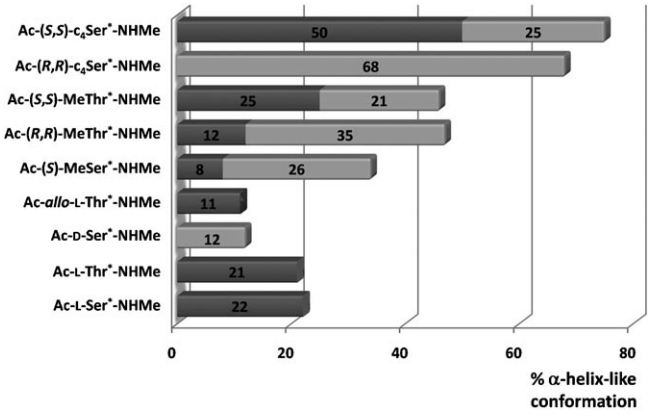

Figure 9. Total helix-like population (dark gray: α_D, light gray: α_L) obtained for the model glycopeptides from the MD-tar simulations.

These results are similar to those obtained for non-glycosylated Ac-D-Ser-NHMe and Ac-*allo*-L-Thr-NHMe (Figure 5) and differ from those previously described for the natural amino acids Ac-L-Ser-NHMe and Ac-L-Thr-NHMe, for which an important increment of the folded conformations were experimentally and theoretically observed for the glycosylated derivatives (Ac-L-Ser*-NHMe and Ac-L-Thr*-NHMe) when compared to the model peptides.[6] On the other hand, although the backbone of Ac-(*S*,*S*)-c_4Ser*-NHMe shows mainly a α_D helical conformation, the backbone of the diastereoisomer Ac-(*R*,*R*)-c_4Ser*-NHMe adopts the contrary helix (α_L helix), which is in accordance with the opposite configuration that both compounds present at the Cα atom. The same feature can be found in derivatives Ac-(*S*,*S*)-MeThr*-NHMe (α_D helix) and Ac-(*R*,*R*)-MeThr*-NHMe (α_L helix).

On the other hand, and as previously observed for Ac-c_4Ser-NHMe, only one ring-puckering conformation of the cyclobutane ring was observed in model glycopeptides Ac-(*S*,*S*)-c_4Ser*-NHMe and Ac-(*R*,*R*)-c_4Ser*-NHMe ($\theta = -31.6$ and 30.0°, respectively). This fact is in good agreement with the Hβ–Hδa distances experimentally determined for these compounds (see the Supporting Information).[23] Moreover, and following the same behavior observed for the model peptide Ac-c_4Ser-NHMe, the glycopeptides present the substituent at the Cβ atom in an equatorial position.

Figure 10 shows the conformational preference of the lateral chain for the model glycopeptides. Concerning the glycopeptides derived from the natural amino acids we previ-

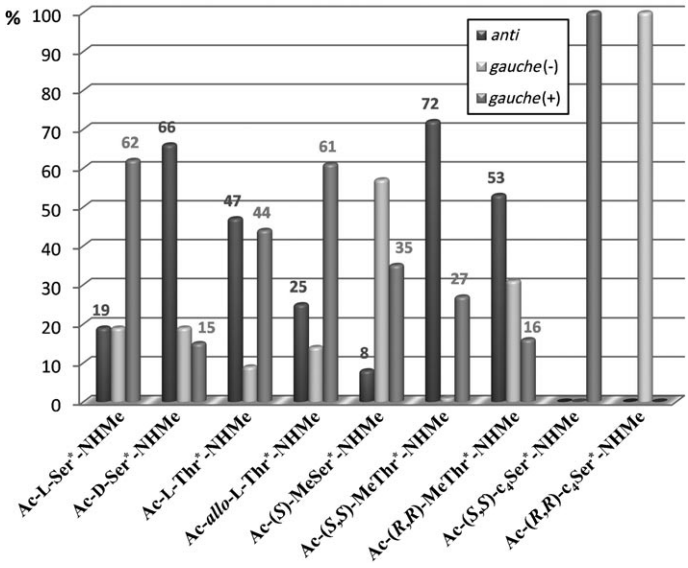

Figure 10. χ^1 distributions obtained from the MD-tar simulations for the different model glycopeptides. Angle χ^1 is around 105 and −105° for Ac-(*S*,*S*)-c_4Ser*-NHMe and Ac-(*R*,*R*)-c_4Ser*-NHMe, respectively.

ously described,[6] whereas the χ^1 dihedral angle in glycopeptide Ac-L-Ser*-NHMe has a similar distribution to the parent peptide Ac-L-Ser-NHMe, glycopeptide Ac-L-Thr*-NHMe differs significantly from Ac-L-Thr-NHMe. Indeed, the lateral chain in Ac-L-Thr*-NHMe mainly adopts the *gauche*(+) and *anti* conformations (44 and 47%, respectively), whereas the *gauche*(+) conformer is mainly populated (72%) in the model peptide Ac-L-Thr-NHMe. A similar feature was observed when Ac-(*S*)-MeSer-NHMe is compared to Ac-(*S*)-MeSer*-NHMe. On the other hand, β-*O*-glucosylation does not significantly affect the lateral chain of the Ac-*allo*-L-Thr-NHMe model peptide. Concerning the α-methylthreonine derivatives, whereas the lateral chain of model peptide Ac-(*S*,*S*)-MeThr-NHMe is totally rigid, with an χ^1 angle of around 180°, the corresponding model glycopeptides Ac-(*S*,*S*)-MeThr*-NHMe and Ac-(*R*,*R*)-MeThr*-NHMe exhibit the three possible conformers but also show a clear preference for the *anti* conformations. Markedly, the rotation around the χ^1 angle in the glycopeptide Ac-D-Ser*-

NHMe is somehow restricted, with a clear preference for the *anti* conformers (close to 70%). Finally, the cyclobutane derivatives Ac-(*S*,*S*)-c_4Ser*-NHMe and Ac-(*R*,*R*)-c_4Ser*-NHMe display, as expected, only one conformer of the lateral chain (Figures 7 and 10).

The conformation of the glycosidic linkage, characterized by the ϕ_s and ψ_s torsional angles, is mainly determined by the exo-anomeric effect,[24] which fixes the value of ϕ_s around −60° in all the derivatives. On the other hand the glycosidic linkage of Ac-D-Ser*-NHMe and Ac-(*S*)-MeSer*-NHMe showed a conformational behavior similar to that observed for Ac-L-Ser*-NHMe (Figure 11), thus indicating that neither the stereochemistry at the Cα atom nor the presence of a methyl group at the Cα atom significantly affect the conformation of the glycosidic linkage in the serine derivatives.

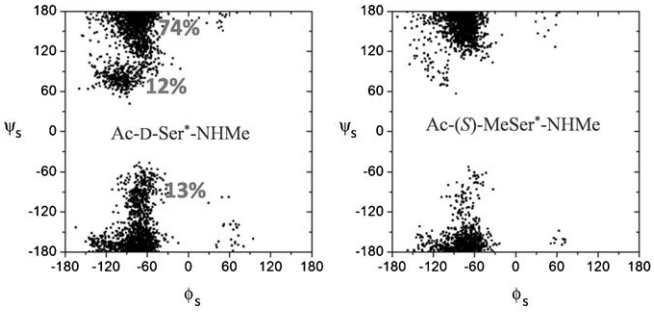

Figure 11. Glycosidic linkage (ϕ_s/ψ_s) distributions obtained from the MD-tar simulations for the model glycopeptides Ac-D-Ser*-NHMe and Ac-(*S*)-MeSer*-NHMe.

On the contrary, the presence of the methyl group at the Cβ atom notably affects the conformation of this linkage. In this sense, we recently reported that the methyl group of Thr forces the ψ_s angle to adopt a value close to 120° for glycopeptides with *N*-acetylgalactosamine. Therefore, the Hβ–Cβ and O1s–C1s bonds are in an eclipsed conformation.[17b] The typical alternate conformation of the ψ_s angle (denoted herein as the *anti* conformation) is drastically destabilized in Ac-L-Thr*-NHMe by steric effects between the H1s atom and the β-methyl group (Figure 12). As a result, this conformation is not populated throughout the MD trajectory.

Consequently, the eclipsed conformer (centered around $\psi_s = 120°$ and denoted as E in Figures 12 and 13) is mainly populated (65%) in Ac-L-Thr*-NHMe. Additionally, a different alternate conformation of the ψ_s angle is present (denoted as *g*(+) in Figures 12 and 13), with ψ_s close to 60°. The *g*(+) conformation of the ψ_s angle is mainly populated when the χ^1 angle has a value close to 180° (Figure 14a). In contrast, the eclipsed conformers show largely a χ^1 value of around 60°.

To determine whether this unexpected result comes from artifacts in the MD simulations (Figure 14), relaxed potential-energy surface (PES) scans at the B3LYP/6-31G(d,p) level were performed on the reduced model of Ac-L-Thr*-NHMe around the ψ_s dihedral angle considering the two

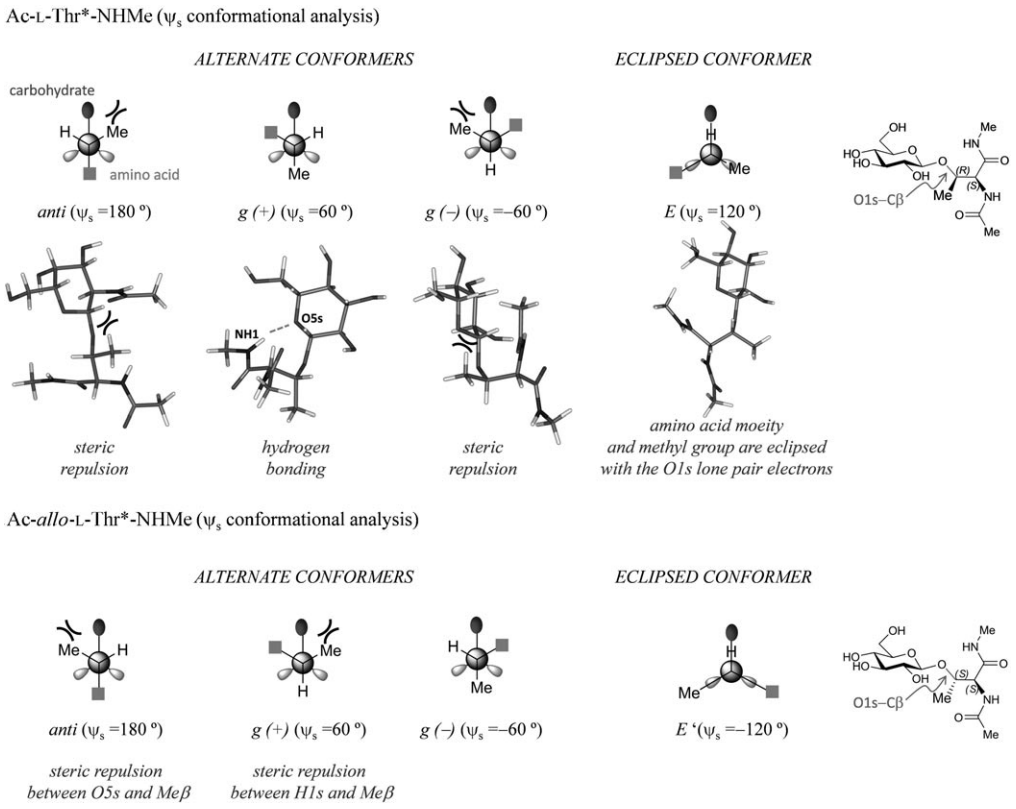

Figure 12. Newman projections of the Cβ–O1s bond of Ac-L-Thr*-NHMe and Ac-*allo*-L-Thr*-NHMe, together with representative 3D structures of each conformation.

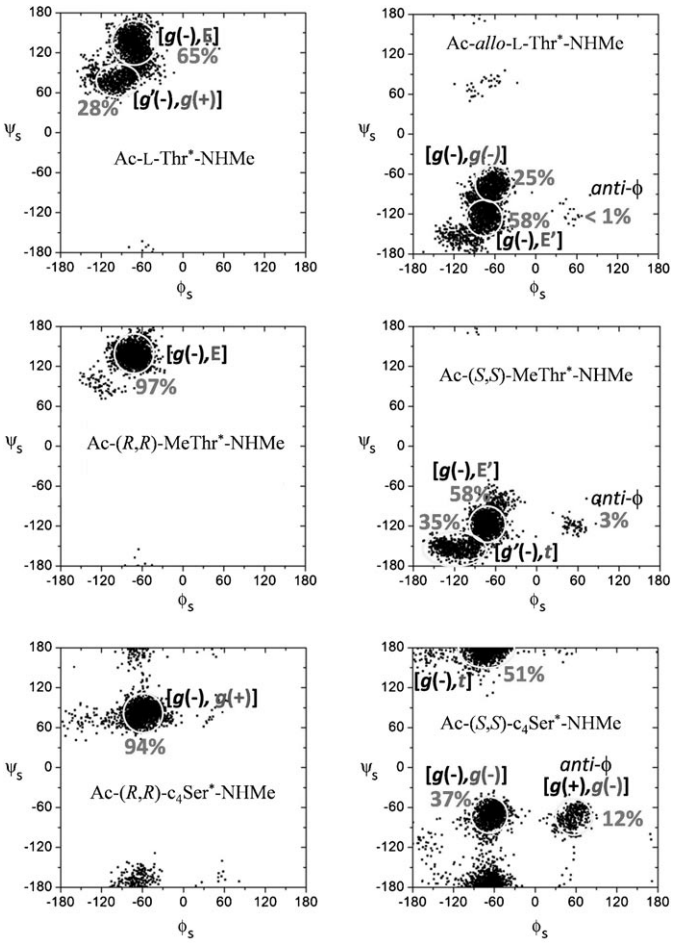

Figure 13. Glycosidic linkage (ϕ_s/ψ_s) distributions obtained from the MD-tar simulations for the model glycopeptides Ac-L-Thr*-NHMe, Ac-*allo*-L-Thr*-NHMe, Ac-(*S*,*S*)-MeThr*-NHMe, Ac-(*R*,*R*)-MeThr*-NHMe, Ac-(*S*,*S*)-c_4Ser*-NHMe, and Ac-(*R*,*R*)-c_4Ser*-NHMe. The *g*(+) conformation of ϕ_s (O5s-C1s-O1s-Cβ = 60°) is also known as *anti*-ϕ (corresponding to 180° when the ϕ_s is defined as H1s-C1s-O1s-Cβ).

major conformations of the χ^1 torsional angle, that is the *anti* and *g*(+) conformations (Figure 15a). As a result, the alternate and eclipsed conformations of ψ_s (*g*(+) and E, respectively) of the reduced model were found as minima-energy rotamers. Interestingly, the *g*(+) conformation of the ψ_s angle is stabilized by a hydrogen bond between the O5s and NH1 atoms (Figure 14). In this sense, the atypical values for ϕ_s (around −100°) presented in this conformation could contribute to optimization of the hydrogen bond. On the other hand, and considering the important role that water molecules play in the conformational preferences of these systems, it is important to mention that this hydrogen-bonding interaction was also found (44% of the total trajectory time) in the unrestrained MD simulations carried out on Ac-L-Thr*-NHMe with explicit water molecules (see Figure 14b and the Supporting Information).

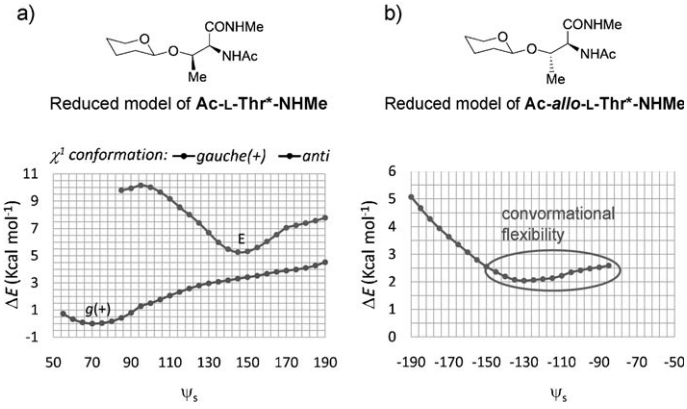

Figure 15. Relaxed PES scan at the B3LYP/6-31G(d,p) level performed with the reduced models of a) Ac-L-Thr*-NHMe and b) Ac-*allo*-L-Thr*-NHMe around the ψ_s dihedral angle. For the reduced model of Ac-L-Thr*-NHMe, the two major conformations of the lateral chain (χ^1) were considered: *g*(+) and *anti*. On the other hand, for the reduced model of Ac-*allo*-L-Thr*-NHMe only the major conformation of the lateral chain (χ^1 close to 60°) was considered in the calculations.

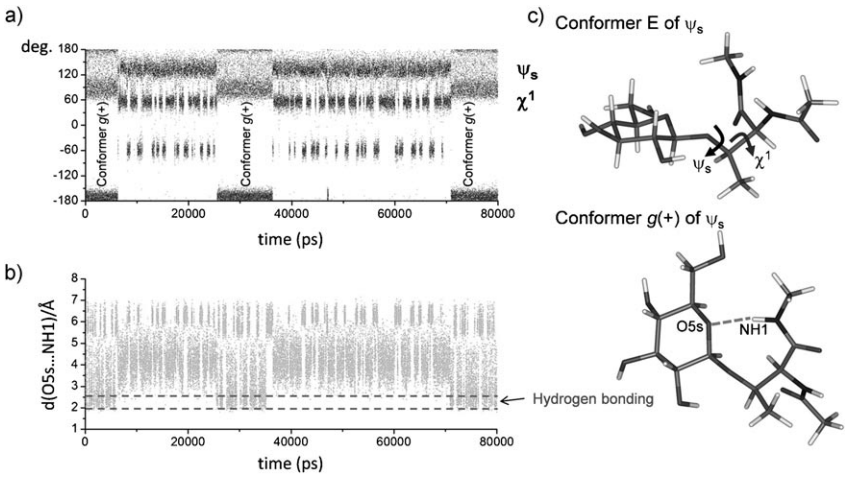

Figure 14. a) Time series monitoring ψ_s and χ^1 dihedral angles during 80 ns MD-tar simulations; b) time series monitoring the distance O5s···NH1; c) 3D structures of conformers E and *g*(+) of ψ_s in Ac-L-Thr*-NHMe.

Some important conclusions can be drawn from the analysis of the glycosidic linkage of the β-methylated compounds with an *S* configuration at the Cβ atom (i.e., Ac-*allo*-L-Thr*-NHMe, Ac-(*S*,*S*)-MeThr*-NHMe, and Ac-(*S*,*S*)-c_4Ser*-NHMe). This configuration of the β-methyl group significantly increases the flexibility of the glycosidic linkage (Figure 13). Indeed, the ψ_s angle has values from −160 to −60° for the acyclic derivatives Ac-*allo*-L-Thr*-NHMe and Ac-(*S*,*S*)-MeThr*-NHMe. This feature is in good agreement with the relaxed PES scan at the B3LYP/6-31G-

(d,p) level performed with the reduced model of Ac-*allo*-L-Thr*-NHMe along the ψ_s dihedral angle, in which a plateau of less 1 Kcal mol^{-1} is observed between these angle values (Figure 15b).

For compounds Ac-*allo*-L-Thr*-NHMe and Ac-(*S*,*S*)-MeThr*-NHMe, the eclipsed conformation of the ψ_s angle (denoted as E′ in Figure 13) is the most populated. Interestingly, an alternate conformation *anti*, with an ψ_s value of around −180° is also present. This conformation shows that the ϕ_s value is close to −120° to avoid the steric contact between the O5s atom and the β-methyl group. Additionally, the *g*(−) conformation of the ψ_s angle could be stabilized by an intramolecular hydrogen bond between the NH2 atom and the O5s and O6s atoms (Figure 16a). Notably, although both the steric repulsion between the β-methyl group and the carbohydrate moiety and the possible hydrogen bonding must play important roles in the unexpected flexibility of the ψ_s angle, the influence of water molecules could also be significant. Indeed, the conformation of Ac-(*S*,*S*)-c_4Ser*-NHMe centered at ϕ_s and ψ_s values of around −60° could be explained in terms of the existence of bridging water molecules between the O2s atom and the carbonyl O1 atom of the peptide backbone, as can be deduced from the corresponding two-dimensional radial-pair distribution function[25] obtained from the unrestrained MD simulation (see Figure 16b and the Supporting Information).

On the other hand, the glycosidic linkage of Ac-(*S*,*S*)-c_4Ser*-NHMe shows a larger degree of mobility not only around ψ_s but also, and more importantly, around the ϕ_s angle. Whereas the most populated conformations exhibit a typical value for the ϕ_s dihedral angle around −60°, there is also a significant population with the ϕ_s value close to 60°. This conformation, which is in accordance with the exo-anomeric effect, is usually referred as an *anti*-ϕ conformation (the ϕ_s values are close to 180° when defined as H1s-C1s-O1s-Cβ; Figure 13). The MD-tar simulations suggest a population of approximately 12% for this unusual conformation. Although the existence of this higher-energy conformation has been experimentally confirmed for some di- and trisaccharides[26] and for oligosaccharides bound to proteins,[27] to the best of our knowledge this case is the first time that an *anti*-ϕ conformation has been experimentally observed in model glycopeptides. The exceptionally large proportion of *anti*-ϕ conformations found for glycopeptide Ac-(*S*,*S*)-c_4Ser*-NHMe was experimentally detected by a medium NOE Hβ–H2s interaction, exclusive of this conformational region. That is, the existence of a short Hβ–H2s average distance (estimated to be 2.9 Å from the NOE interaction build-up curves) can never be explained without assuming the existence of the *anti*-ϕ population (the Hβ–H2s distance in a *syn* conformation is longer than 4.5 Å; Figure 17).

This relatively large proportion of the *anti*-ϕ conformers in aqueous solution could be stabilized by the formation of intramolecular hydrogen bonds. Indeed, there is a strong correlation between the *anti*-ϕ conformation and the existence of two simultaneous hydrogen bonds, between the NH1 and O5s atoms and the NH1 and O6s atoms. The behavior of the glycosidic linkage of Ac-(*S*,*S*)-c_4Ser*-NHMe was also observed in the unrestrained MD simulations carried out in explicit water (Figure 18). Finally, the *anti*-ϕ conformation was also experimentally detected for Ac-*allo*-L-Thr-NHMe and Ac-(*S*,*S*)-MeThr*-NHMe (Figure 13), that is, for compounds with an *S*,*S* configuration at the Cα and Cβ atoms. However, the population of this conformation is less than 4% in both cases (Figure 13), which is in accordance with the distance of H2s–Hβ deduced from the NOE interaction build-up curves (3.7 and 3.4 Å for Ac-*allo*-L-Thr*-NHMe and Ac-(*S*,*S*)-MeThr*-NHMe, respectively).

Summary of the conformational study of model peptides and glycopeptides: It is well known that the preferred con-

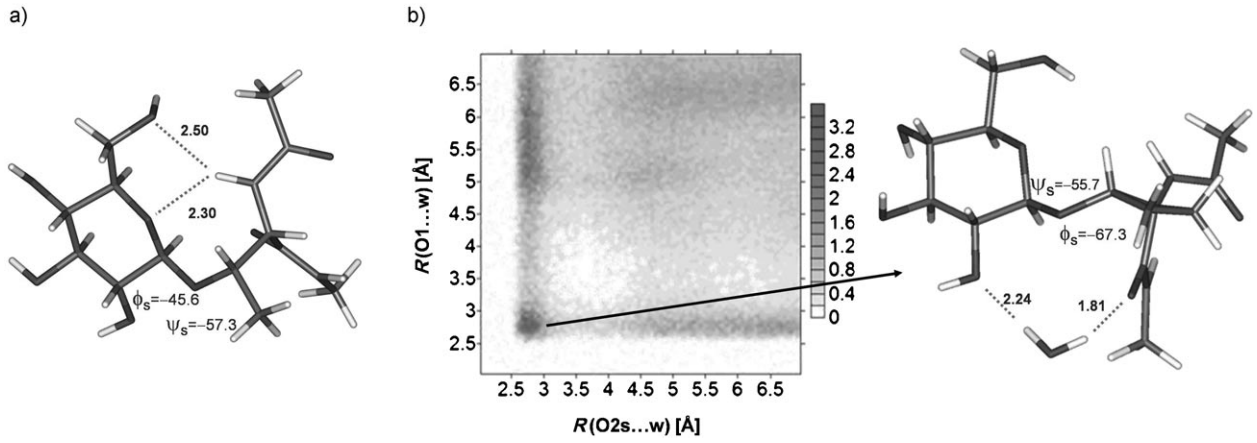

Figure 16. a) Calculated B3LYP/6-31G(d,p) geometry for the conformer *g*(−) conformation of ψ_s in Ac-*allo*-L-Thr*-NHMe. b) Two-dimensional radial-pair distribution function of O1 and O2s and a representative frame of the 20 ns unrestrained MD simulation of Ac-(*S*,*S*)-c_4Ser*-NHMe showing a bridging water molecule (the distances are given in Ångströms and dihedral angles in degrees). The maximum density of this shared water site was 2.5 times greater than the bulk density, with maximum and average residence times of 25.0 and 1.99 ps, respectively. The average distance between O2s and O1 was 5.3 Å, ranging from 2.5 to 7.2 Å.

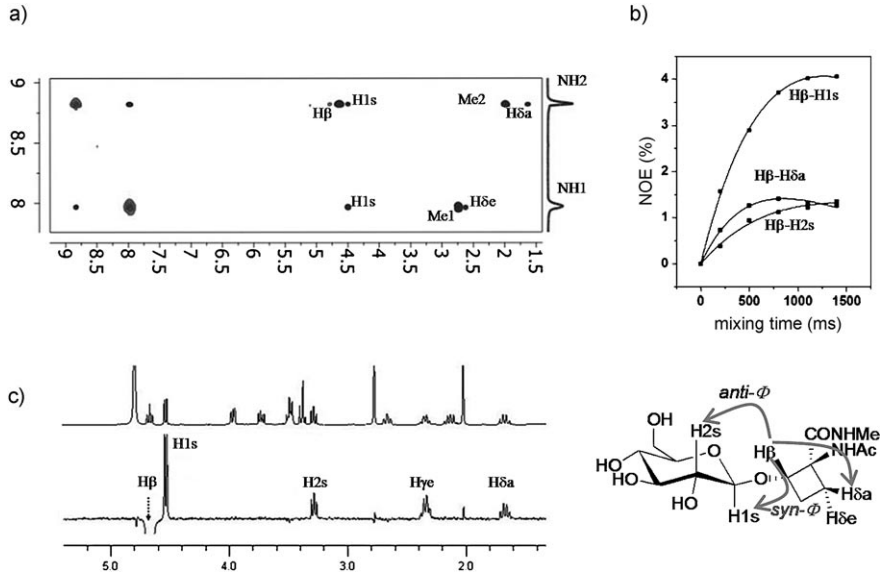

Figure 17. a) The 800 ms 2D NOESY spectrum (400 MHz) of Ac-(*S*,*S*)-c$_4$Ser*-NHMe in H_2O/D_2O (9:1) at 25 °C and pH 4.8. The diagonal peaks are negative. The NOE interactions are represented as positive cross-peaks. b) NOE interaction build-up curves that correspond to the Hβ atom of Ac-(*S*,*S*)-c$_4$Ser*-NHMe (upper panel) and schematic representation of the characteristic NOE interactions of *syn*- and *anti*-ϕ conformations (lower panel). c) Selective 1D NOESY experiments with the 1D-DPFGSE NOESY pulse sequence, which corresponds to the inversion of the Hβ atom in derivative Ac-(*S*,*S*)-c$_4$Ser*-NHMe (a 1D spectrum of this molecule is also shown in the upper part of the figure).

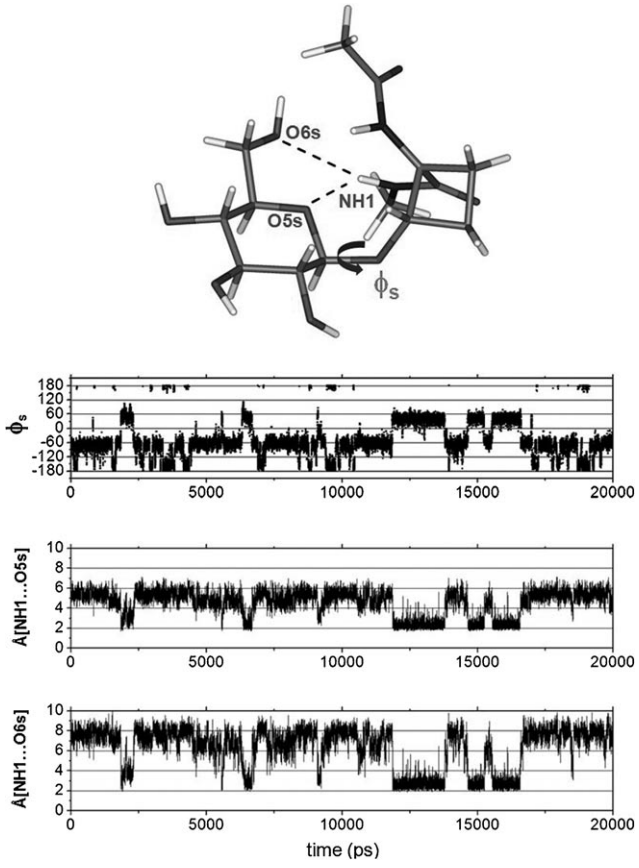

Figure 18. Time series monitoring the ϕ_s dihedral angle and distances NH1···O5s and NH1···O6s in a 20 ns unrestrained MD simulation in explicit water for Ac-(*S*,*S*)-c$_4$Ser*-NHMe.

formations of the backbone of model peptide derived from Ser diamide (Ac-L-Ser-NHMe) in aqueous solution are extended conformations. Additionally, the lateral chain (χ^1 dihedral angle) has a great flexibility, thus showing the coexistence of the *g*(+), *g*(−), and *anti* conformers, with the former being the most populated.[6]

Herein, we have demonstrated that the incorporation of substituents at the Cα or Cβ atoms of Ac-L-Ser-NHMe can modulate both the conformation of the backbone and lateral chain. Therefore, whereas the incorporation of a methyl group at the Cβ position of Ac-L-Ser-NHMe in *S* or *R* configurations mainly does not affect the backbone, this group rigidifies the lateral chain, which clearly prefers the *g*(+) conformation (compare Ac-L-Ser-NHMe with Ac-L-Thr-NHMe and Ac-*allo*-L-Thr-NHMe in Figures 5 and 7). On the other hand, the incorporation of the methyl group at the Cα position of Ac-L-Ser-NHMe or Ac-L-Thr-NHMe promotes the appearance of folded conformations of the backbone. Additionally, the methyl group at the Cβ position (MeThr) drastically rigidifies the χ^1 dihedral angle, thus modulating its values toward the *anti* conformation (compare Ac-L-Ser-NHMe and Ac-L-Thr-NHMe with Ac-(*S*,*S*)-MeThr-NHMe in Figure 7). Moreover, the restriction imposed by the incorporation of a cyclobutane ring into the structure of Ser largely promotes helix-like conformations of the backbone and it makes the *g*(+) conformation exclusive for the lateral chain (compare Ac-L-Ser-NHMe with Ac-c$_4$Ser-NHMe in Figures 5 and 7). These results are summarized in Table 1.

On the other hand, we have studied how β-*O*-glucosylation affects the conformational preference of the backbone and the lateral chain in the above-discussed model peptides. As a result, although the incorporation of a β-*O*-glucose unit into the non-natural α- or β-substituted β-hydroxy-α-amino acids does not significantly affect the backbone conformation, glycosylation promotes an important increment of folded conformations in the natural amino acids Ac-L-Ser-NHMe and Ac-L-Thr-NHMe[6] (compare Figures 5 and 9). Concerning the lateral chain, glycosylation does not affect the conformational space, except for Ac-L-Thr*-NHMe and Ac-(*S*)-MeSer*-NHMe. In the former, glycosylation makes the χ^1 dihedral angle more flexible, thus promoting the shift from the *g*(+) toward the *anti* conformation. For Ac-(*S*)-MeSer*-NHMe, there is a restriction around the χ^1 angle, with a clear preference for *g*(−) conformations

Table 1. Exploration of the conformational space of Ser diamide derivatives that incorporate substituents at the Cα and/or Cβ positions.

Entry	Group incorporated in Ser unit	Position of the group	Configuration Cα,Cβ	Ac-Xxx-NHMe	Backbone ϕ_p/ψ_p	Lateral chain χ^1
1	–	–	*S*,–	L-Ser	folded (7%)	flexible *anti*, *g*(+), *g*(−)
2	CH_3–	β	*S*,*R*	L-Thr	folded (9%)	very rigid *g*(+) (72%)
3	CH_3–	β	*S*,*S*	*allo*-L-Thr	folded (11%)	very rigid *g*(+) (70%)
4	CH_3–	α	*S*,–	MeSer	folded (44%)	flexible *anti*, *g*(+), *g*(−)
5	CH_3–	α,β	*S*,*S*	MeThr	folded (55%)	very rigid *anti* (100%)
6	−CH_2CH_2–	α,β	*S*,*S*	c_4Ser	folded (71%)	very rigid close to *g*(+) (100%)

(compare Figures 7 and 10). It is important to note that β-*O*-glucosylation of Ac-D-Ser-NHMe principally induces an *anti* conformation of the lateral chain.

The most important conclusions are related to the conformation of the glycosidic linkage and particularly with the ψ_s dihedral angle, since the ϕ_s dihedral angle adopts a typical value of −60°, *g*(−) conformation, determined by the exo-anomeric effect in most of the glycopeptides. Interestingly, the only remarkable feature concerning the ϕ_s dihedral angle involves the appearance of a significant amount of the unusual *anti*-ϕ conformation, experimentally observed mainly in the case of Ac-(*S*,*S*)-c_4Ser*-NHMe, which is stabilized by intramolecular hydrogen bonding.

The ψ_s values are strongly dependent on the substitution at the Cα or Cβ atoms: 1) The absence of substituents at the Cβ position of a glucosylated β-hydroxy-α-amino acid (i.e., Ac-L-Ser*-NHMe, Ac-D-Ser*-NHMe, and Ac-(*S*)-MeSer*-NHMe) forces the ψ_s angle to adopt the usual *anti* conformation. 2) The presence of a methyl group at the Cβ position at an *R* configuration of the amino acid (i.e., Ac-L-Thr*-NHMe) does not favor the alternate conformations of ψ_s *anti* and *g*(−); therefore, this substitution gives preference to the *g*(+) alternate conformation and, surprisingly, to the eclipsed (E) conformation (120°). 3) A similar situation occurs when the methyl group at the Cβ position of an amino acid (i.e., Ac-*allo*-L-Thr*-NHMe) is placed in the *S* configuration; in this case, the *anti* and *g*(+) alternate conformations are not favored, whereas *g*(−) alternate and eclipsed (E′; ψ_s close to −120°) conformations of the ψ_s angle are preferred. 4) When the Cα and Cβ positions of an amino acid are substituted at *R*,*R* configurations, the ψ_s dihedral angle is rigidified toward the eclipsed conformer in the case of Ac-(*R*,*R*)-MeThr*-NHMe and toward a *g*(+) alternate conformer in the case of Ac-(*R*,*R*)-c_4Ser*-NHMe. 5) On the contrary and unexpectedly, when the Cα and Cβ positions are substituted at *S*,*S* configurations (i.e., Ac-(*S*,*S*)-MeThr*-NHMe and Ac-(*S*,*S*)-c_4Ser*-NHMe) the ψ_s dihedral angle is made more flexible toward several conformations.

Finally, it is important to highlight that structural rigidity is not a synonym of conformational rigidity. For example, Ac-(*S*,*S*)-c_4Ser*-NHMe and Ac-(*R*,*R*)-c_4Ser*-NHMe are structurally rigid molecules, whereas Ac-(*R*,*R*)-c_4Ser*-NHMe exhibits its large conformational stiffness and its diastereoisomer Ac-(*S*,*S*)-c_4Ser*-NHMe displays a great flexibility towards the glycosidic linkage and a significant rigidity at the amino acid moiety. Logically, these inherent properties (flexibility and/or rigidity) must be taken into account in the analysis of glycopeptide structures and in the interaction of these compounds with other types of molecules (Table 2).

Conclusion

In summary, the incorporation of α- and/or β-substituted β-hydroxy-α-amino acids in model β-*O*-glucopeptides is a powerful tool to design and modulate the conformational space of the different synthesized glycopeptides. In this sense, the expansion of these novel small systems to larger glycopeptidic systems will be considered in future to design derivatives that could stabilize a bioactive conformation or could show conformers that are rarely observed in the natural compounds, thus modifying the binding to the target molecules.

Experimental Section

General procedures: The solvents were purified according to standard procedures. Analytical TLC was performed using Polychrom SI F254 plates. Column chromatography was performed on silica gel 60 (230–400 mesh). ^{1}H and ^{13}C NMR spectra were recorded on Bruker ARX 300 and Bruker Avance 400 spectrometers. ^{1}H and ^{13}C NMR spectra were recorded in $CDCl_3$ with trimethylsilane (TMS) as the internal standard and in D_2O at 25 °C (chemical shifts are reported in ppm on the δ scale and the coupling constants are given in hertz). Melting points were determined on a Büchi B-545 melting-point apparatus and are uncorrected. Optical rotations were measured on a Perkin-Elmer 341 polarimeter. Microanalyses were carried out on a CE Instruments EA-1110 analyzer and are in good agreement with the calculated values. Compound **2** was synthesized from **1** according to a procedure reported in reference [13] and compound **7** was synthesized according a procedure reported in reference [10j].

Compound 3: A solution of **2** (150 mg, 0.26 mmol) in ethyl acetate (10 mL) was hydrogenolyzed by using 10% Pd/C (70 mg) as a catalyst at 25 °C for 16 h. The catalyst and solvent were removed, and the residue corresponding to **3** (113 mg, 90%) was used without any purification. ^{1}H NMR (400 MHz, $CDCl_3$): δ = 1.43 (s, 3H), 1.99 (s, 3H), 2.01 (s, 3H), 2.04 (s, 3H), 2.08 (s, 3H), 3.64 (d, J = 10.4 Hz, 1H), 3.67–3.73 (m, 1H), 4.07–4.19 (m, 2H), 4.24 (dd, J = 4.4, 12.4 Hz, 1H), 4.63 (d, 1H J = 7.8 Hz), 4.97 (dd, J = 8.1, 9.0 Hz, 1H), 5.09 ("t", J = 9.6 Hz, 1H), 5.20 ppm ("t", J = 9.4 Hz, 1H); ^{13}C NMR (100 MHz, $CDCl_3$): δ = 19.8,

Table 2. Exploration of the conformational space of β-*O*-Glc-Ser diamide derivatives that incorporate substituents at the Cα and/or Cβ positions.

Entry	Group incorporated in Ser	Position of the group	Configuration Cα,Cβ	Compound Ac-Xxx*-NHMe	Backbone ϕ_p/ψ_p	Lateral chain χ^1	Glycosidic linkage ϕ_s	Glycosidic linkage ψ_s
1	–	–	*S*,–	L-Ser*	folded (22%)	rigid *g*(+) (62%)	rigid *g*(−)	*anti* with flexibility
2	CH_3–	β	*S*,*R*	L-Thr*	folded (21%)	flexible *g*(+), *anti*	rigid *g*(−)	rigid *g*(+), E
3	–	–	*R*	D-Ser*	folded (12%)	rigid *anti* (66%)	rigid *g*(−)	*anti* with flexibility
4	CH_3–	β	*S*,*S*	*allo*-L-Thr*	folded (11%)	rigid *g*(+) (61%)	rigid *g*(−)	rigid *g*(−), E′
5	CH_3–	α	*S*,–	MeSer*	folded (34%)	flexible *g*(−), *g*(+)	rigid *g*(−)	*anti* with flexibility
6	CH_3–	α,β	*S*,*S*	MeThr*	folded (46%)	flexible *anti*, *g*(+)	rigid *g*(−)	rigid *anti*, E′
7	CH_3–	α,β	*R*,*R*	MeThr*	folded (47%)	flexible *anti*, *g*(−)	rigid *g*(−)	rigid E
8	$-CH_2CH_2-$	α,β	*S*,*S*	c_4Ser*	folded (75%)	very rigid close to *g*(+) (100%)	flexible *g*(−), *g*(+)[a]	flexible *anti*, *g*(−)
9	$-CH_2CH_2-$	α,β	*R*,*R*	c_4Ser*	folded (68%)	very rigid close to *g*(−) (100%)	rigid *g*(−)	rigid *g*(+)

[a] *g*(+) conformation of the ϕ_s angle (O5 s-C1 s-O1 s-Cβ = 60°) is also so-called *anti*-ϕ (corresponding to 180° when the ϕ_s angle is defined as H1 s-C1 s-O1 s-Cβ).

20.5, 20.6, 20.7, 21.0, 61.8, 66.0, 68.3, 71.0, 71.8, 72.6, 74.1, 100.8, 169.5, 169.7, 170.3, 170.9, 174.0 ppm.

Compound 4: A solution of **3** (109 mg, 0.23 mmol) in acetonitrile (5 mL) was treated with diisopropylethylamine (DIPEA; 0.2 mL, 1.5 mmol), methylamine hydrochloride (29 mg, 0.46 mmol), and TBTU (90 mg, 0.27 mmol) under an inert atmosphere. The reaction mixture was stirred at 25 °C for 16 h and then partitioned between water (5 mL) and ethyl acetate (5 mL). The organic layer was washed with 0.5 N HCl (1 × 15 mL) and brine (1 × 15 mL). The aqueous phase was extracted with $CHCl_3$/*i*PrOH (3:1, 1 × 15 mL). The organic layer was dried over anhydrous Na_2SO_4, filtered, and evaporated to give a residue that was purified by column chromatography on silica gel eluting with CH_2Cl_2/MeOH (9:1) to yield **4** as a white oil (94 mg, 84%). ^{1}H NMR (400 MHz, $CDCl_3$): δ = 1.53 (s, 3H), 2.01 (s, 3H), 2.03 (s, 3H), 2.07 (s, 3H), 2.09 (s, 3H), 2.81 (d, J = 4.2 Hz, 3H), 3.68–3.75 (m, 2H), 4.08–4.17 (m, 2H), 4.25 (dd, J = 4.7, 12.4 Hz, 1H), 4.56 (d, J = 7.9 Hz, 1H), 5.03 (dd, J = 7.9, 9.5 Hz, 1H), 5.09 ("t", J = 9.7 Hz, 1H), 5.22 ("t", J = 9.5 Hz, 1H), 6.59–6.67 ppm (m, 1H); ^{13}C NMR (100 MHz, $CDCl_3$): δ = 19.1, 20.6, 20.6, 20.6, 20.7, 26.4, 61.8, 66.4, 68.3, 71.2, 71.9, 72.6, 73.8, 100.9, 169.4, 169.4, 170.2, 170.2, 170.7 ppm; elemental analysis calcd (%) for $C_{19}H_{28}N_4O_{11}$: C 46.72, H 5.78, N 11.47; found: C 46.59, H 5.84, N 11.32.

Compound 5: A solution of methylamide **4** (94 mg, 0.19 mmol) in MeOH (10 mL) was hydrogenated using 10% Pd/C (40 mg) as a catalyst at 25 °C for 15 h. The catalyst and solvent were removed, and the residue was used without any purification. The crude product was dissolved in pyridine (3 mL) and acetic anhydride (1 mL) was added. The resulting mixture was stirred for 4 h at 25 °C. The solvent was evaporated and the crude produce purified by column chromatography on silica gel eluting with CH_2Cl_2/MeOH (95:5) to yield **5** (74 mg, 77%). ^{1}H NMR (400 MHz, $CDCl_3$): δ = 1.56 (s, 3H), 2.00 (s, 3H), 2.01 (s, 3H), 2.03 (s, 3H), 2.06 (s, 3H), 2.11 (s, 3H), 2.80 (d, J = 4.8 Hz, 3H), 3.71 (ddd, J = 2.3, 4.8, 10.0 Hz, 1H), 3.86 (d, J = 9.9 Hz, 1H), 4.12 (dd, J = 2.2, 12.4 Hz, 1H), 4.29–4.36 (m, 2H), 4.52 (d, J = 8.0 Hz, 1H), 5.00 (dd, J = 8.0, 9.7 Hz, 1H), 5.07 ("t", J = 9.7 Hz, 1H), 5.22 ("t", J = 9.5 Hz, 1H), 6.65 (br s 1H), 6.75–6.81 ppm (m, 1H); ^{13}C NMR (100 MHz, $CDCl_3$): δ = 20.3, 20.5, 20.6, 24.1, 25.3, 26.5, 59.5, 61.6, 68.2, 71.2, 71.5, 71.9, 72.3, 100.5, 169.4, 169.6, 170.0, 170.4, 170.6, 172.9 ppm; elemental analysis calcd (%) for $C_{21}H_{32}N_2O_{12}$: C 50.00, H 6.39, N 5.55; found: C 49.89, H 6.32, N 5.59.

Ac-(*S*)-MeSer*-NHMe: A solution of **5** (52 mg, 0.10 mmol) in MeOH (5 mL) was treated with MeONa/MeOH (0.5 M) to pH 9. The reaction mixture was stirred for 3 h and then neutralized with Dowex 50W-X8, filtered, and concentrated. Purification of the residue with a C_{18} reverse-phase sep-pak cartridge gave the desired model glycopeptide Ac-(*S*)-MeSer*-NHMe (31 mg, 90%). $[\alpha]_D^{29} = -23.7$ (c = 0.6, MeOH); ^{1}H NMR (400 MHz, D_2O): δ = 1.36 (s, 3H), 1.89 (s, 3H), 2.60, (s, 3H), 3.18 (dd, J = 8.1, 9.3 Hz, 1H), 3.23 ("t", J = 9.6 Hz, 1H), 3.30–3.34 (m, 1H), 3.37 ("t", J = 9.1 Hz, 1H), 3.60 (dd, J = 5.6, 12.3 Hz, 1H), 3.71 (d, J = 10.2 Hz, 1H), 3.79 (dd, J = 1.9, 12.3 Hz, 1H), 4.04 (d, J = 10.2 Hz,1H), 4.34 ppm (d, J = 7.9 Hz, 1H); ^{13}C NMR (100 MHz, D_2O): δ = 19.8, 22.2, 26.0, 59.5, 60.7, 69.6, 72.2, 73.0, 75.6, 75.9, 102.7, 173.8, 174.8 ppm; elemental analysis calcd (%) for $C_{13}H_{24}N_2O_8$: C 46.42, H 7.19, N 8.33; found: C 46.54, H 7.11, N 8.39.

Ac-(*R*,*R*)-MeThr*-NHMe: A solution of **6** (52 mg, 0.06 mmol) in MeOH (5 mL) was treated with MeONa/MeOH (0.5 M) to pH 9. The reaction mixture was stirred for 3 h at 25 °C and then neutralized with Dowex 50-X8, filtered, and concentrated. Purification of the residue with C_{18} reverse-phase sep-pak cartridge gave Ac-(*R*,*R*)-MeThr*-NHMe as a colorless oil (21 mg, 87%). $[\alpha]_D^{25} = +4.2$ (c = 0.97, H_2O); ^{1}H NMR (400 MHz, D_2O): δ = 1.19 (d, J = 6.4 Hz, 3H), 1.45 (s, 3H), 1.99 (s, 3H), 2.72 (s, 3H), 3.29–3.36 (m, 1H), 3.43–3.55 (m, 3H), 3.82 (dd, J = 4.5, 12.1 Hz, 1H), 3.94–3.99 (m, 1H), 4.12 (q, J = 6.4 Hz, 1H), 4.51 ppm (d, J = 7.9 Hz, 1H); ^{13}C NMR (100 MHz, D_2O): δ = 14.1, 18.3, 22.4, 26.0, 60.5, 62.2, 69.4, 72.7, 75.6, 75.9, 78.0, 100.6, 173.4, 173.6 ppm; elemental analysis calcd (%) for $C_{14}H_{26}N_2O_8$: C 47.99, H 7.48, N 8.00. found: C 48.11, H 7.52, N 7.94.

Compound 8: LiOH·H_2O (265 mg, 6.3 mmol) was added to a solution of **7** (350 mg, 1.3 mmol) in H_2O/MeOH (1:3, 8 mL) at 25 °C. After the reaction mixture was stirred at 25 °C for 12 h, the MeOH was evaporated, and the reaction mixture diluted with H_2O (20 mL) and ethyl acetate (25 mL). The aqueous phase was acidified with 2 N HCl and extracted with $CHCl_3$/*i*PrOH (3:1, 3 × 15 mL). The combined organic phases were dried over Na_2SO_4 and the solvent was removed at reduced pressure to give the corresponding amino acid derivative **8** as a white solid (320 mg, 97%), which was used without further purification in the next step. ^{1}H NMR (400 MHz, CD_3OD): δ = 1.60 ("q", J = 10.5 Hz, 1H), 1.96 (s, 3H), 2.12–2.25 (m, 2H), 2.70–2.78 (m, 1H), 4.30 ("t", J = 8.4 Hz, 1H), 4.48 (d, J = 11.1 Hz, 1H), 4.66 (d, J = 11.1 Hz, 1H), 7.26–7.32 ppm (m, 5H); ^{13}C NMR (100 MHz, CD_3OD): δ = 22.2, 25.6, 25.7, 67.0, 72.8, 78.8, 128.7, 128.9, 129.3, 139.3, 172.8, 173.9 ppm.

Compound 9: A solution of acid **8** (620 mg, 2.4 mmol) in acetonitrile (30 mL) was treated with DIPEA (1.56 mL, 9.4 mmol), methylamine hydrochloride (318 mg, 4.7 mmol), and TBTU (908 mg, 2.8 mmol) under an inert atmosphere. The reaction mixture was stirred at 25 °C for 10 h, then partitioned between brine (20 mL) and ethyl acetate (12 mL). The organic layer was washed with 0.1 N HCl (2×15 mL) and 5% $NaHCO_3$ (2×15 mL). The aqueous layer was then extracted with $CHCl_3$/*i*PrOH (4:1, 3×20 mL). Finally, the combined organic layers were dried over Na_2SO_4, filtered, and evaporated to give a residue that was purified by column chromatography on silica gel eluting with ethyl acetate/MeOH (95:5) to give **9**, as a white solid (600 mg, 92%). M.p. 172–174 °C; ^{1}H NMR (400 MHz, $CDCl_3$): δ = 1.82–1.95 (m, 4H), 1.99–2.09 (m, 1H), 2.11–2.28 (m, 2H), 2.78 (d, J = 4.7 Hz, 3H), 4.49 (d, J = 11.5 Hz, 1H), 4.56–4.69 (m, 2H), 6.39 (brs, 1H), 7.22–7.33 (m, 5H), 7.40 ppm (m, 1H); ^{13}C NMR (100 MHz, $CDCl_3$): δ = 23.8, 24.1, 24.5, 26.4, 64.7, 72.2, 78.1, 128.0, 128.0, 128.5, 137.6, 170.1, 172.3 ppm; elemental analysis calcd (%) for $C_{15}H_{20}N_2O_3$: C 65.20, H 7.30, N 10.14; found: C 65.33, H 7.25, N 10.20.

Ac-c$_4$Ser-NHMe: A solution of **9** (600 mg, 2.2 mmol) in MeOH (20 mL) was hydrogenolyzed using 10% Pd/C (100 mg) as a catalyst at 25 °C for 12 h. The catalyst and solvent were removed and further purification of the residue with C_{18} reverse-phase sep-pak cartridge gave c$_4$Ser as a white solid (400 mg, 99%). ^{1}H NMR (400 MHz, D_2O): δ = 1.51–1.67 (m, 1H), 1.85–2.01 (m, 4H), 2.18–2.35 (m, 1H), 2.48–2.63 (m, 1H), 2.73 (s, 3H), 4.34 ppm ("t", J = 8.7 Hz, 1H); ^{13}C NMR (100 MHz, D_2O): δ = 21.8, 23.8, 26.0, 26.1, 65.9, 71.2, 172.8, 173.9 ppm; elemental analysis calcd (%) for $C_8H_{14}N_2O_3$: C 51.60, H 7.58, N 15.04; found: C 51.71, H 7.62, N 15.10.

Compounds 10 and 11: Silver triflate (262 mg, 1.0 mmol) was added to a suspension of c$_4$Ser (115 mg, 0.6 mmol) and powdered molecular sieves (4 Å, 50 mg) in dichloromethane (4 mL) in an inert atmosphere. The reaction mixture was stirred at −30 °C and then 2,3,4,6-tetra-*O*-benzoyl-α-D-glucopyranosyl bromide (570 mg, 0.86 mmol) in dichloromethane (4 mL) was added. The reaction mixture was stirred at this temperature for 1 h, warmed to 25 °C, and stirred for additional 14 h. The crude product was filtered, concentrated, and purified by column chromatography on silica gel eluting with CH_2Cl_2/MeOH (95:5) to give a mixture of **10** and **11** as a white solid (140 mg, 30%). Additional column chromatography eluting with CH_2Cl_2/MeOH (95:5) allowed us to obtain **11** (55 mg) and **10** (34 mg) in a pure form.

10: M.p. 100–102 °C; $[\alpha]_D^{25}$ = +22.4 (c = 1.12, MeOH); ^{1}H NMR (400 MHz, $CDCl_3$): δ = 1.71–1.84 (m, 1H), 1.89 (s, 3H), 1.97–2.09 (m, 1H), 2.21–2.35 (m, 2H), 2.42 (d, J = 4.5 Hz, 3H), 4.11–4.20 (m, 1H), 4.49–4.65 (m, 2H), 4.73–4.83 (m, 1H), 5.20 (d, J = 8.0 Hz, 1H), 5.55 (dd, J = 8.3, 9.5 Hz, 1H), 5.65 ("t", J = 9.7 Hz, 1H), 5.94 ("t", J = 9.7 Hz, 1H), 6.37 (brs, 1H), 6.85–6.99 (m, 1H), 7.22–7.31 (m, 2H), 7.32–7.47 (m, 7H), 7.47–7.61 (m, 3H), 7.77–7.85 (m, 2H), 7.88–7.94 (m, 2H), 7.96–8.07 ppm (m, 4H); ^{13}C NMR (100 MHz, $CDCl_3$): δ = 23.4, 24.3, 26.0, 26.1, 63.0, 64.7, 71.7, 72.4, 72.7, 76.9, 77.2, 100.2, 128.3, 128.4, 128.7, 128.8, 129.7, 133.2, 134.4, 134.5, 165.2, 165.5, 165.6, 166.1, 169.9, 171.4 ppm; elemental analysis calcd (%) for $C_{42}H_{40}N_2O_{12}$: C 65.96, H 5.27, N 3.66; found: C 65.82, H 5.33, N 3.60.

11: M.p. 128–130 °C; $[\alpha]_D^{25}$ = +11.0 (c = 1.07, MeOH); ^{1}H NMR (400 MHz, $CDCl_3$): δ = 1.87–1.93 (m, 1H), 1.98 (s, 3H), 2.03–2.22 (m, 2H), 2.34–2.45 (m, 1H), 2.64 (d, J = 4.7 Hz, 3H), 4.12–4.19 (m, 1H), 4.36 (dd, J = 4.2, 12.3 Hz, 1H), 4.84 (dd, J = 2.6, 12.3 Hz, 1H), 4.92 (d, J = 8.0 Hz, 1H), 4.97 ("t", J = 8.6 Hz, 1H), 5.43 (dd, J = 8.1, 9.7 Hz, 1H), 5.71 ("t", J = 9.8 Hz, 1H), 5.90 ("t", J = 9.7 Hz, 1H), 6.58 (brs, 1H), 6.63–6.69 (m, 1H), 7.24–7.63 (m, 12H), 7.79–7.86 (m, 2H), 7.89–7.96 (m, 4H), 8.05–8.11 ppm (m, 2H); ^{13}C NMR (100 MHz, $CDCl_3$): δ = 23.6, 23.7, 24.4, 26.4, 62.2, 65.6, 69.1, 71.8, 72.5, 72.8, 76.8, 77.2, 100.4, 128.3, 128.5, 128.6, 128.7, 129.7, 133.3, 133.5, 133.6, 165.1, 165.3, 165.7, 166.3, 170.2, 170.8 ppm; elemental analysis calcd (%) for $C_{42}H_{40}N_2O_{12}$: C 65.96, H 5.27, N 3.66; found: C 66.10, H 5.21, N 3.71.

Ac-(*S*,*S*)-c$_4$Ser*-NHMe: A solution of **10** (38 mg, 0.05 mmol) in MeOH (5 mL) was treated with MeONa/MeOH (0.5 M) to pH 9. The reaction mixture was stirred for 3 h at 25 °C and was then neutralized with Dowex 50-X8, filtered, and concentrated. Purification of the residue with a C_{18} reverse-phase sep-pak cartridge gave Ac-(*S*,*S*)-c$_4$Ser*-NHMe as a colorless oil in (16 mg, 92%). $[\alpha]_D^{25}$ = −7.2 (c = 1.24, H_2O); ^{1}H NMR (400 MHz, D_2O): δ = 1.59–1.73 (m, 1H), 2.01 (s, 3H), 2.06–2.19 (m, 1H), 2.28–2.39 (m, 1H), 2.60–2.71 (m, 1H), 2.77 (s, 3H), 3.28 ("t", J = 8.5 Hz, 1H), 3.34–3.40 (m, 1H), 3.44–3.53 (m, 2H), 3.72 (dd, J = 6.7, 12.2 Hz, 1H), 3.92–4.00 (m, 1H), 4.53 (d, J = 7.9 Hz, 1H), 4.66 ppm ("t", J = 8.8 Hz, 1H); ^{13}C NMR (100 MHz, D_2O): δ = 21.8, 24.4, 25.1, 26.1, 60.9, 65.4, 69.8, 72.7, 75.4, 75.5, 76.1, 100.8, 172.3, 173.7 ppm; elemental analysis calcd (%) for $C_{14}H_{24}N_2O_8$: C 48.27, H 6.94, N 8.04; found: C 48.17, H 6.88, N 8.10.

Ac-(*R*,*R*)-c$_4$Ser*-NHMe: A solution of **11** (60 mg, 0.08 mmol) in MeOH (5 mL) was treated with MeONa/MeOH (0.5 M) to pH 9. The reaction mixture was stirred for 3 h at 25 °C and then neutralized with Dowex 50-X8, filtered, and concentrated. Purification of the residue with C_{18} reverse-phase sep-pak cartridge gave Ac-(*R*,*R*)-c$_4$Ser*-NHMe as a colorless oil (23 mg, 85%). $[\alpha]_D^{25}$ = −16.1 (c = 1.17, H_2O); ^{1}H NMR (400 MHz, D_2O): δ = 1.56–1.68 (m, 1H), 2.00 (s, 3H), 2.07–2.15 (m, 1H), 2.26–2.39 (m, 1H), 2.66–2.79 (m, 4H), 3.23 ("t", J = 8.5 Hz, 1H), 3.35–3.41 (m, 1H), 3.44–3.56 (m, 2H), 3.78 (dd, J = 6.0, 12.0 Hz, 1H), 3.99 (dd, J = 2.0, 12.0 Hz, 1H), 4.40 ("t", J = 8.9 Hz, 1H), 4.47 ppm (d, J = 7.8 Hz, 1H); ^{13}C NMR (100 MHz, D_2O): δ = 21.8, 24.1, 24.7, 26.1, 60.7, 66.0, 69.7, 73.0, 75.5, 75.5, 77.6, 101.3, 172.6, 173.5 ppm; elemental analysis calcd (%) for $C_{14}H_{24}N_2O_8$: C 48.27, H 6.94, N 8.04; found: C 48.40, H 7.00, N 7.98.

Compound 12: EDCI·HCl (80 mg, 0.4 mmol) and DMAP (9 mg, 0.08 mmol) were added to a suspension of acid **8** (100 mg, 0.38 mmol) in dichloromethane (5 mL) in an inert atmosphere. The reaction mixture was stirred for 2 h at 25 °C and then concentrated and purified by column chromatography silica gel eluting with hexane/ethyl acetate (2:3) to give **12** as an oil (80 mg, 87%). ^{1}H NMR (400 MHz, $CDCl_3$): δ = 1.95–2.12 (m, 4H), 2.12–2.32 (m, 2H), 2.33–2.53 (m, 1H), 4.26–4.46 (m, 2H), 4.48–4.62 (m, 1H), 7.23–7.42 ppm (m, 5H); ^{13}C NMR (100 MHz, $CDCl_3$): δ = 14.8, 22.8, 24.1, 71.7, 73.6, 78.0, 127.6, 127.7, 128.1, 137.2, 162.3, 176.6 ppm; elemental analysis calcd (%) for $C_{14}H_{15}NO_3$: C 68.56, H 6.16, N 5.71; found: C 68.68, H 6.21, N 5.67.

Compounds 13 and 14: *t*BuOK (0.3 mL, 0.3 mmol) was added to a solution of (*S*)-(−)-1-(2-naphtyl)ethanol (100 mg, 0.6 mmol) in THF (3 mL) in an inert atmosphere. After the reaction mixture was stirred for 5 min at 25 °C, a solution of oxazolone **12** (72 mg, 0.3 mmol) in THF (3 mL) was added. The reaction mixture was further stirred for 12 h at 25 °C and then was concentrated and purified by column chromatography on silica gel eluting with hexane/ethyl acetate (2:3) to give a mixture of **13** and **14** (85 mg, 70%). Further purification by column chromatography on silica gel eluting with hexane/ethyl acetate (2:3) allowed pure **14** (7 mg, 6%) to be obtained with an additional mixture fraction with **13** and **14** in a ratio of 1:4 (17 mg, 14%).

14: M.p. 133–135 °C; $[\alpha]_D^{25}$ = −81.4 (c = 1.00, MeOH); ^{1}H NMR (400 MHz, $CDCl_3$): δ = 1.58 (d, J = 6.6 Hz, 3H), 1.86 (s, 3H), 2.17–2.33 (m, 3H), 2.33–2.52 (m, 1H), 4.33–4.47 (m, 2H), 4.56–4.71 (m, 1H), 6.04–6.30 (m, 2H), 7.12–7.25 (m, 5H), 7.36–7.50 (m, 3H), 7.70–7.82 ppm (m, 4H); ^{13}C NMR (100 MHz, $CDCl_3$): δ = 21.9, 22.6, 23.8, 24.6, 66.4, 71.6, 74.2, 77.2, 124.0, 125.0, 126.1, 126.2, 127.6, 127.8, 127.9, 128.0, 128.3, 128.4, 133.0, 133.1, 137.7, 138.4, 169.8, 170.7 ppm; elemental analysis calcd (%) for $C_{26}H_{27}NO_4$: C 74.80, H 6.52, N 3.35; found: C 74.69, H 6.46, N 3.40.

Compound (*R*,*R*)-8: LiOH·H_2O (126 mg, 3.0 mmol) was added to a solution of a mixture of **13** and **14** in a ratio of 1:4 (84 mg, 0.2 mmol) in H_2O/MeOH (1:3, 4 mL) at 25 °C. After the reaction mixture was stirred at 25 °C for four days, the MeOH was evaporated, and the reaction mixture diluted with H_2O (3 mL) and ethyl acetate (5 mL). The aqueous phase was acidified with 2 N HCl and extracted with $CHCl_3$/*i*PrOH (3:1, 4×5 mL). The combined organic phases were dried over Na_2SO_4 and the solvent was removed at reduced pressure to give a white solid corresponding to a mixture of enantiomers (*S*,*S*)- and (*R*,*R*)-**8** in a ratio of 1:4, respectively (51 mg, 96%). The spectroscopic data are identical to those obtained for racemic compound **8**.

Two-dimensional NMR experiments: NMR spectroscopic experiments were recorded on a Bruker Avance 400 spectrometer at 293 K. Magnitude-mode ge-2D COSY spectra were recorded with gradients using the cosygpqf pulse program with a 90° pulse width. Phase-sensitive ge-2D HSQC spectra were recorded using a z-filter and selection before t1 to remove the decoupling during acquisition by use of the invigpndph pulse program with CNST2 (JHC) = 145. Two-dimensional NOESY experiments were made using phase-sensitive ge-2D NOESY with WATER-

GATE for spectra in H_2O/D_2O (9:1). Selective ge-1D NOESY experiments were carried out using the 1D-DPFGE NOE pulse sequence. NOE interaction intensities were normalized with respect to the diagonal peak at zero mixing time. Experimental NOE interactions were fitted to a double exponential function, $f(t)=p_0(e^{-p_1t})(1-e^{-p_2t})$ with p_0, p_1, and p_2 as adjustable parameters.[18] The initial slope was determined from the first derivative at time $t=0$, $f'(0)=p_0p_2$. From the initial slopes, interproton distances were obtained by employing the isolated spin-pair approximation. 1D NOESY (D_2O) and 2D NOESY (H_2O/D_2O, 9:1) spectra for model peptides and glycopeptides and the representative NOE interaction build-up curves are available in the Supporting Information.

Computational details

Molecular mechanics calculations: Relaxed potential-energy maps were calculated by performing relaxed 2D-PES scans of the ϕ_p and ψ_p dihedrals. A grid of 400 conformers was constructed for each structure by fully scanning these torsions with a step size of 18°. The AMBER94,[28] CHARMM,[29] and MM+[30] force fields were used in the minimizations. In the case of AMBER94 and CHARMM, a distance-independent dielectric constant of 80 was used. No cut-offs were introduced for the nonbonded interactions. A Fletcher–Reeves conjugate gradient algorithm was used in minimizations with a root-mean square gradient of 0.01 kcal Å^{-1} mol^{-1} or 2000 cycles as the convergence criteria. The relative energy levels were plotted from 0.0 to 1.6 kcal mol^{-1} with a contour spacing of 0.4 kcal mol^{-1}.

Molecular dynamics simulations: MD-tar simulations were performed with AMBER[31] 6.0 (AMBER94), which was implemented with GLYCAM04 parameters[32] to accurately simulate the conformational behavior of the sugar moiety. Additionally, in the case of cyclobutane derivatives the General Amber Force Field[33] (GAFF) was used in the simulations. Distances derived from NOE interactions were included as time-averaged distance constraints, and scalar coupling constants J as time-averaged coupling constraints. A $<r^{-6}>^{-1/6}$ average was used for the distances and a linear average was used for the coupling constants. Final trajectories were run using an exponential decay constant of 8000 ps and a simulation length of 80 ns with a dielectric constant $\varepsilon=80$. The distances derived experimentally and from MD simulations calculated for all the peptides and glycopeptides and the ϕ_p/ψ_p distributions obtained from the MD-tar simulations for the glycopeptides and MD simulations in explicit water for Ac-L-Thr*-NHMe and Ac-(*S*,*S*)-c$_4$Ser*-NHMe are available in the Supporting Information.

Density functional theory (DFT) calculations: All calculations were carried out using the B3LYP hybrid functional[34] with the Gaussian 03 package.[35] The 6-31G(d,p) basis set was used in the full optimizations and for the relaxed PES scans. In these calculations, a step size of 5° was used. Basis set superposition error corrections were not considered in this study. Frequency analyses were carried out at the same level used in the geometry optimizations, and the nature of the stationary points was determined in each case according to the appropriate number of negative eigenvalues of the Hessian matrix. Scaled frequencies were not considered since significant errors in the calculated thermodynamical properties are not found at this theoretical level.[36] B3LYP/6-31G(d,p) coordinates of the optimized $g(-)$ conformer of Ac-*allo*-L-Thr*-NHMe are available in the Supporting Information.

X-ray diffraction analysis[37]

Crystal data for Ac-c$_4$Ser-NHMe: $C_8H_{14}N_2O_3$, $M_w=186.21$, colorless prism of $0.25\times0.25\times0.15$ mm, $T=173$ K, monoclinic, space group $P2_1/c$, $Z=4$, $a=8.0203(4)$, $b=17.5720(9)$, $c=6.8646(3)$ Å, $\beta=92.123(3)$°, $V=966.78(8)$ Å^3, $\rho_{calcd}=1.279$ g cm^{-3}, $F(000)=400$, $\lambda=0.71073$ Å ($Mo_{K\alpha}$), $\mu=0.098$ mm^{-1}, Nonius kappa CCD diffractometer, θ range = 2.54–27.91°, 7579 collected reflections, 2275 unique, full-matrix least-squares (SHELXL97),[38] $R_1=0.0672$, $\omega R_2=0.1969$, ($R_1=0.1195$, $\omega R_2=0.2294$ all data), goodness of fit = 1.068, residual electron density = 0.379–−0.327 e Å^{-3}; the hydrogen atoms were fitted at theoretical positions.

*Crystal data for **14***: $C_{26}H_{27}NO_4$, $M_w=417.51$, colorless prism of $0.40\times0.20\times0.04$ mm, $T=173$ K, orthorhombic, space group $P2_12_12_1$, Z = 4, $a=5.8415(2)$, $b=15.3797(7)$, $c=24.8256(12)$ Å, $V=2230.3$ (2) Å^3, $\rho_{calcd}=1.243$ g cm^{-3}, $F(000)=888$, $\lambda=0.71073$ Å ($Mo_{K\alpha}$), $\mu=0.083$ mm^{-1}, Nonius kappa CCD diffractometer, θ range = 1.56–23.50°, 7469 collected reflections, 3272 unique, full-matrix least-squares (SHELXL97),[38] $R_1=0.0590$, $\omega R_2=0.1102$, ($R_1=0.0933$, $\omega R_2=0.1246$ all data), goodness of fit = 1.073, residual electron density = 0.278–0.215 e Å^{-3}; the hydrogen atoms were fitted at theoretical positions.

Acknowledgements

We thank the Ministerio de Educación y Ciencia and FEDER (project CTQ2006–05825/BQU, Ramón y Cajal contracts for F.C., J.H.B., and a pre-doctoral grant for A.F.-T.). G.J.-O. thanks the Consolider Project (Ingenio 2010) for financial support, We also thank CESGA for computer support.

[1] a) R. A. Dwek, *Chem. Rev.* **1996**, *96*, 683–720; b) A. Varki, *Glycobiology* **1993**, *3*, 97–130; c) D. H. Williams, *Nat. Prod. Rep.* **1996**, *13*, 469–478; d) D. F. Wyss, G. Wagner, *Curr. Opin. Biotechnol.* **1996**, *7*, 409–416; e) T. Buskas, S. Ingale, G.-J. Boons, *Glycobiology* **2006**, *16*, 113R-136R; f) C. R. Bertozzi, L. L. Kiessling, *Science* **2001**, *291*, 2357–2364; g) M. R. Pratt, C. R. Bertozzi, *Chem. Soc. Rev.* **2005**, *34*, 58–68.

[2] a) P. Van den Steen, P. M. Rudd, R. A. Dwek, G. Opdenakker, *Crit. Rev. Biochem. Mol. Biol.* **1998**, *33*, 151–208; b) H. C. Hang, C. R. Bertozzi, *Bioorg. Med. Chem.* **2005**, *13*, 5021–5034.

[3] G. W. Hart, M. P. Housley, C. Slawson, *Nature* **2007**, *446*, 1017–1022.

[4] a) L. Shao, Y. Luo, D. J. Moloney, R. S. Haltiwanger, *Glycobiology* **2002**, *12*, 763–770; b) R. J. Harris, M. W. Spellman, *Glycobiology* **1993**, *3*, 219–224.

[5] K. Bruckner, L. Perez, H. Clausen, S. Cohen, *Nature* **2000**, *406*, 411–415.

[6] F. Corzana, J. H. Busto, S. B. Engelsen, J. L. Asensio, J. Jiménez-Barbero, J. M. Peregrina, A. Avenoza, *Chem. Eur. J.* **2006**, *12*, 7864–7871.

[7] a) C. Cativiela, M. D. Díaz-de-Villegas, *Tetrahedron: Asymmetry* **1998**, *9*, 3517–3599; b) C. Cativiela, M. D. Díaz-de-Villegas, *Tetrahedron: Asymmetry* **2000**, *11*, 645–732; c) C. Cativiela, M. D. Díaz-de-Villegas, *Tetrahedron: Asymmetry* **2007**, *18*, 569–623; d) H. Vogt, S. Bräse, *Org. Biomol. Chem.* **2007**, *5*, 406–430.

[8] a) M. Wilstermann, L. O. Kononov, U. Nilsson, A. K. Ray, G. Magnusson, *J. Am. Chem. Soc.* **1995**, *117*, 4742–4754; b) R. Alibés, D. R. Bundle, *J. Org. Chem.* **1998**, *63*, 6288–6301; c) A. Geyer, M. Müller, R. R. Schmidt, *J. Am. Chem. Soc.* **1999**, *121*, 6312–6313.

[9] J. W. Lane, R. L. Halcomb, *J. Org. Chem.* **2003**, *68*, 1348–1357.

[10] a) A. Avenoza, C. Cativiela, F. Corzana, J. M. Peregrina, M. M. Zurbano, *Tetrahedron: Asymmetry* **2000**, *11*, 2195–2204; b) A. Avenoza, C. Cativiela, F. Corzana, J. M. Peregrina, D. Sucunza, M. M. Zurbano, *Tetrahedron: Asymmetry* **2001**, *12*, 949–957; c) A. Avenoza, J. I. Barriobero, J. H. Busto, C. Cativiela, J. M. Peregrina, *Tetrahedron: Asymmetry* **2002**, *13*, 625–632; d) A. Avenoza, J. I. Barriobero, C. Cativiela, M. A. Fernández-Recio, J. M. Peregrina, F. Rodríguez, *Tetrahedron* **2001**, *57*, 2745–2755; e) A. Avenoza, J. H. Busto, C. Cativiela, J. M. Peregrina, D. Sucunza, M. M. Zurbano, *Tetrahedron: Asymmetry* **2003**, *14*, 399–405; f) A. Avenoza, J. H. Busto, F. Corzana, J. M. Peregrina, D. Sucunza, M. M. Zurbano, *Tetrahedron: Asymmetry* **2004**, *15*, 719–724; g) A. Avenoza, J. H. Busto, F. Corzana, J. M. Peregrina, D. Sucunza, M. M. Zurbano, *Synthesis* **2005**, 575–578; h) A. Avenoza, J. H. Busto, N. Canal, J. M. Peregrina, *Chem. Commun.* **2003**, 1376–1377; i) A. Avenoza, J. H. Busto, N. Canal, J. M. Peregrina, *J. Org. Chem.* **2005**, *70*, 330–333; j) A. Avenoza, J. H. Busto, N. Canal, J. M. Peregrina, M. Pérez-Fernández, *Org. Lett.* **2005**, *7*, 3597–3600; k) C. Aydillo, G. Jiménez-Osés, J. H. Busto, J. M. Peregrina, M. M. Zurbano, A. Avenoza, *Chem. Eur. J.* **2007**, *13*, 4840–4848; l) G. Jiménez-Osés, C. Aydillo, J. H. Busto, M. M. Zurbano, J. M. Peregrina, A. Avenoza, *J. Org. Chem.* **2007**, *72*, 5399–5402.

[11] S. Gnanakaran, A. E. García, *J. Phys. Chem. B* **2003**, *107*, 12555–12557.
[12] S. Hanessian, J. Banoub, *Carbohydr. Res.* **1977**, *53*, C13–C16.
[13] A. Avenoza, J. M. Peregrina, E. San Martín, *Tetrahedron Lett.* **2003**, *44*, 6413–6416.
[14] a) H. J. Dyson, P. E. Wright, *Annu. Rev. Anthropol. Annu. Rev. Biophys. Chem.* **1991**, *20*, 519–538; b) H. J. Dyson, P. E. Wright, *Annu. Rev. Phys. Chem.* **1996**, *47*, 369–395.
[15] The letter code was employed in S. S. Zimmerman, M. S. Pottle, G. Nemethy, H. A. Scheraga, *Macromolecules* **1977**, *10*, 1–9; therein, the β conformer is referred to as E, the PPII as F, and the α-helix conformation as A.
[16] D. A. Cumming, J. P. Carver, *Biochemistry* **1987**, *26*, 6664–6676.
[17] a) F. Corzana, J. H. Busto, G. Jiménez-Osés, J. L. Asensio, J. Jiménez-Barbero, J. M. Peregrina, A. Avenoza, *J. Am. Chem. Soc.* **2006**, *128*, 14640–14648; b) F. Corzana, J. H. Busto, G. Jiménez-Osés, M. García de Luis, J. L. Asensio, J. Jiménez-Barbero, J. M. Peregrina, A. Avenoza, *J. Am. Chem. Soc.* **2007**, *129*, 9458–9467.
[18] T. Haselhorst, T. Weimar, T. Peters, *J. Am. Chem. Soc.* **2001**, *123*, 10705–10714.
[19] a) A. Marco, M. Llinas, K. Wuthrich, *Biopolymers* **1978**, *17*, 617–636; b) G. W. Vuister, A. Bax, *J. Am. Chem. Soc.* **1993**, *115*, 7772–7777.
[20] D. A. Pearlman, *J. Biomol. NMR* **1994**, *4*, 1–16.
[21] D. Obrecht, M. Altorfer, C. Lehmann, P. Schonholzer, K. Muller, *J. Org. Chem.* **1996**, *61*, 4080–4086.
[22] a) V. N. Balaji, K. Ramnarayan, M. F. Chan, S. N. Rao, *Peptide Res.* **1995**, *8*, 178–186; b) M. Gatos, F. Formaggio, M. Crisma, C. Toniolo, G. M. Bonora, Z. Benedetti, B. Di Blasco, R. Iacovino, A. Santini, M. Saviano, J. Kamphuis, *J. Pept. Sci.* **1997**, *3*, 110–122.
[23] a) G. Jiménez-Osés, F. Corzana, J. H. Busto, M. Pérez-Fernández, J. M. Peregrina, A. Avenoza, *J. Org. Chem.* **2006**, *71*, 1869–1878; b) A. Avenoza, J. H. Busto, N. Canal, J. M. Peregrina in *Structural Analysis of Cyclic Systems* (Ed.: I. Iriepa), Research Signpost, T.C., Kerala (India), **2005**, pp. 55–68.
[24] G. R. J. Thatcher, *The Anomeric Effect and Associated Stereoelectronic Effects*, American Chemical Society, Washington, DC **1993**.
[25] C. Andersson, S. B. Engelsen, *J. Mol. Graphics J. Mol. Graph. Model.* **1999**, *17*, 101–105.
[26] a) J. Dabrowski, T. Kozár, H. Grosskurth, N. E. Nifant'ev, *J. Am. Chem. Soc.* **1995**, *117*, 5534–5539; b) C. Landersjö, R. Stenutz, G. Widmalm, *J. Am. Chem. Soc.* **1997**, *119*, 8695–8698; c) R. Bukowski, L. M. Morris, R. J. Woods, T. Weimar, *Eur. J. Org. Chem.* **2001**, *7*, 2697–2705; d) C. Höög, C. Landersjö, G. Widmalm, *Chem. Eur. J.* **2001**, *7*, 3069–3077; e) K. Lycknert, A. Helander, S. Oscarson, L. Kenne, G. Widmalm, *Carbohydr. Res.* **2004**, *339*, 1331–1338.
[27] C. A. Bush, M. Martín-Pastor, A. Imberty, *Ann. Rev. Biophys. Biomol. Struct.* **1999**, *28*, 269–293.
[28] W. D. Cornell, P. C. Cieplack, I. Bayly, I. R. Gould, K. Merz, D. M. Ferguson, D. C. Spellmeyer, T. Fox, J. W. Caldwell, P. A. Kollman, *J. Am. Chem. Soc.* **1995**, *117*, 5179–5197.
[29] N. Foloppe, A. D. MacKerell, Jr., *J. Comp. Chem.* **2000**, *21*, 86–104.
[30] a) N. Allinger, *J. Am. Chem. Soc.* **1977**, *99*, 8127–8134; b) N. Allinger, X. Zhou, J. Bergsma, *J. Mol. Struct.* **1994**, *312*, 69–83.
[31] a) D. A. Pearlman, D. A. Case, J. W. Caldwell, W. R. Ross, T. E. Cheatham III, S. DeBolt, D. Ferguson, G. Seibel, P. A. Kollman, *Comput. Phys. Commun.* **1995**, *91*, 1–41; b) AMBER 6, D. A. Case, D. A. Pearlman, J. W. Caldwell, T. E. Cheatham, III, W. S. Ross, C. L. Simmerling, T. A. Darden, K. M. Merz, R. V. Stanton, A. L. Cheng, J. J. Vincent, M. Crowley, V. Tsui, R. J. Radmer, Y. Duan, J. Pitera, I. Massova, G. L. Seibel, U. C. Singh, P. K. Weiner, P. A. Kollman, University of California, San Francisco, **1999**.
[32] R. J. Woods, R. A. Dwek, C. J. Edge, B. Fraser-Reid, *J. Phys. Chem.* **1995**, *99*, 3832–3846.
[33] J. Wang, R. M. Wolf, J. W. Caldwell, P. A. Kollman, D. A. Case, *J. Comput. Chem.* **2004**, *25*, 1157–1174.
[34] a) C. Lee, W. Yang, R. Parr, *Phys. Rev. B* **1988**, *37*, 785–789; b) A. D. Becke, *J. Chem. Phys.* **1993**, *98*, 5648–5652.
[35] Gaussian 03, Revision C.01, M. J. Frisch, G. W. Trucks, H. B. Schlegel, G. E. Scuseria, M. A. Robb, J. R. Cheeseman, J. A. Montgomery, Jr., T. Vreven, K. N. Kudin, J. C. Burant, J. M. Millam, S. S. Iyengar, J. Tomasi, V. Barone, B. Mennucci, M. Cossi, G. Scalmani, N. Rega, G. A. Petersson, H. Nakatsuji, M. Hada, M. Ehara, K. Toyota, R. Fukuda, J. Hasegawa, M. Ishida, T. Nakajima, Y. Honda, O. Kitao, H. Nakai, M. Klene, X. Li, J. E. Knox, H. P. Hratchian, J. B. Cross, C. Adamo, J. Jaramillo, R. Gomperts, R. E. Stratmann, O. Yazyev, A. J. Austin, R. Cammi, C. Pomelli, J. W. Ochterski, P. Y. Ayala, K. Morokuma, G. A. Voth, P. Salvador, J. J. Dannenberg, V. G. Zakrzewski, S. Dapprich, A. D. Daniels, M. C. Strain, O. Farkas, D. K. Malick, A. D. Rabuck, K. Raghavachari, J. B. Foresman, J. V. Ortiz, Q. Cui, A. G. Baboul, S. Clifford, J. Cioslowski, B. B. Stefanov, G. Liu, A. Liashenko, P. Piskorz, I. Komaromi, R. L. Martin, D. J. Fox, T. Keith, M. A. Al-Laham, C. Y. Peng, A. Nanayakkara, M. Challacombe, P. M. W. Gill, B. Johnson, W. Chen, M. W. Wong, C. Gonzalez, J. A. Pople, Gaussian, Inc., Wallingford CT, **2004**.
[36] C. W. Bauschlicher, Jr., *Chem. Phys. Lett.* **1995**, *246*, 40–44.
[37] CCDC-681037 (Ac-c_4Ser-NHMe) and CCDC-681036 (**14**) contain the supplementary crystallographic data for this paper. These data can be obtained free of charge from The Cambridge Crystallographic Data Centre via www.ccdc.cam.ac.uk/data_request/cif
[38] G. M. Sheldrick, SHELXL97, Program for the refinement of crystal structures, University of Göttingen, Germany, **1997**.

Received: March 13, 2008
Revised: April 23, 2008
Published online: July 4, 2008

